Escola de Camins
Escola Tècnica Superior d'Enginyeria de Camins, Canals i Ports
UPC BARCELONATECH

TREBALL FINAL DE GRAU

A continuous-discontinuous model to introduce fluid pressure in a crack

Treball realitzat per:
Montserrat Casado-Antolín

Dirigit per:
Antonio Rodríguez-Ferran

Grau en:
Enginyeria Civil

Barcelona, juny de 2016

Departament d'Enginyeria Civil i Ambiental

Abstract

A continuous-discontinuous model to introduce fluid pressure in a crack

Montserrat Casado-Antolín

In recent years, combined continuous-discontinuous models are starting to be used to simulate failure processes of quasi-brittle materials –concrete or rocks, for instance. Merging the strong points of both the continuous and discontinuous model, allows a better characterisation of the whole failure process.

The goal of this thesis is to present a new contribution on this direction. The main concern of this work is to introduce a fluid pressure in the crack that will cause crack opening. This contribution is focused on the discontinuous part of the problem, once the macroscopic crack is generated.

First, the eXtended Finite Element Method (X-FEM) is used to introduce a discontinuity in the displacement field. To this end, nodal enrichment of the cracked elements is discussed. Then, the pressure term p is analysed. Its contribution only appears in the discontinuous part of the displacement field, that is the components corresponding to the enriched degrees of freedom.

Once the technique is elaborated, it is applied to an elastic bulk with different cracks. An appropriate treatment of the nodal enrichment and the computation of nodal forces, provide consistent results of crack opening and bulk deformation. Furthermore, propagation of the crack, element-by-element, is developed in the elastic bulk, obtaining progressive crack opening.

Finally, the proposed technique is applied to a damageable bulk with different cracks. In order to overcome pathological mesh-sensitivity, regularisation techniques must be applied. The appropriate boundary conditions for the regularisation problem and the damage model are discussed. Finally, several examples show the damage field caused by the pressure.

Graphical abstract

A continuous-discontinuous model to introduce fluid pressure in a crack

Montserrat Casado-Antolín

X-FEM: discontinuous displacement field

$$\mathbf{u}(\mathbf{x}) = \mathbf{u}^1(\mathbf{x}) + \psi(\mathbf{x})\mathbf{u}^2(\mathbf{x})$$

$$\psi(\mathbf{x}) = \begin{cases} -1 & \text{if} \quad \mathbf{x} \in \Omega^- \\ 1 & \text{if} \quad \mathbf{x} \in \Omega^+ \end{cases}$$

ELASTIC BULK $\boldsymbol{\sigma = E\varepsilon}$

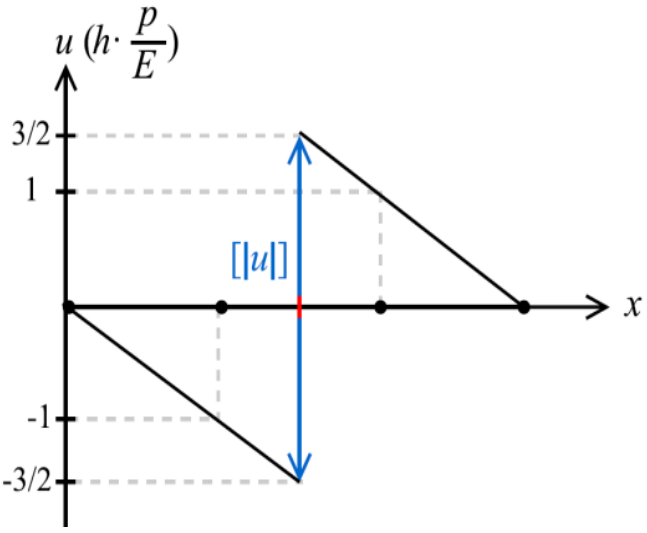

Propagation

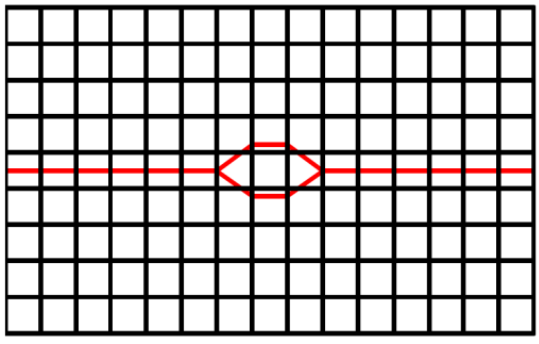

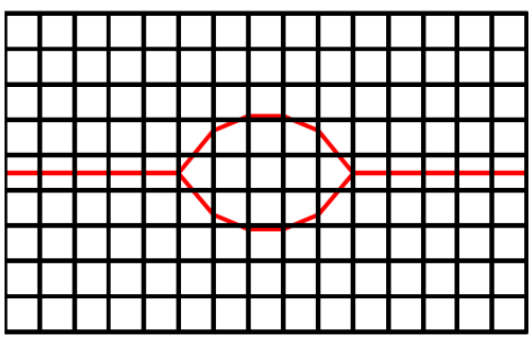

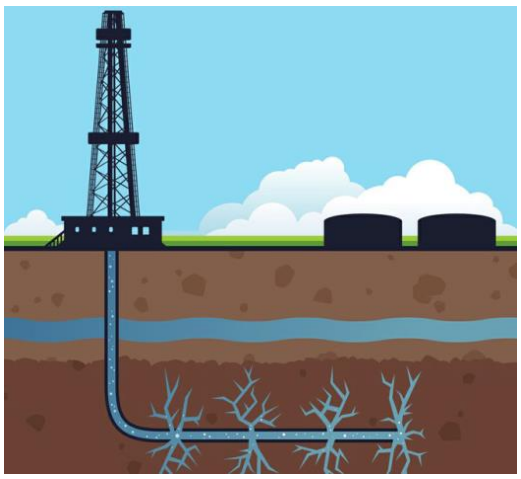

Hydraulic fracture

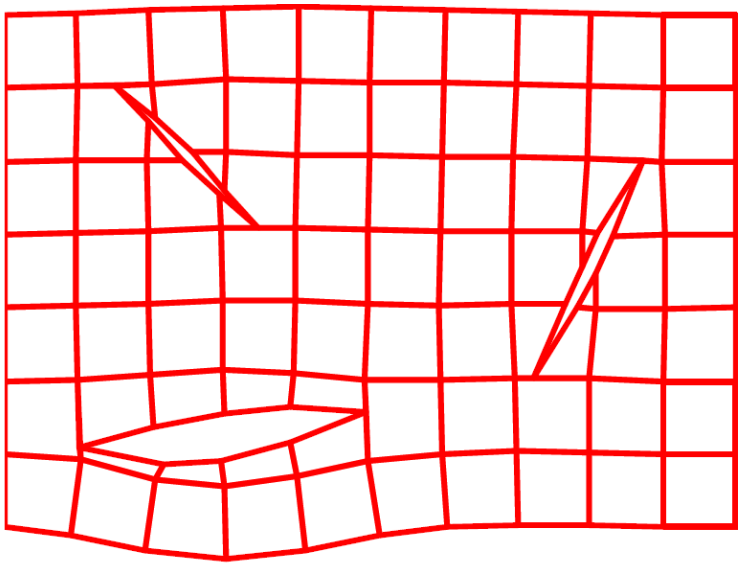

DAMAGEABLE BULK $\boldsymbol{\sigma = (1 - D)E\varepsilon}$

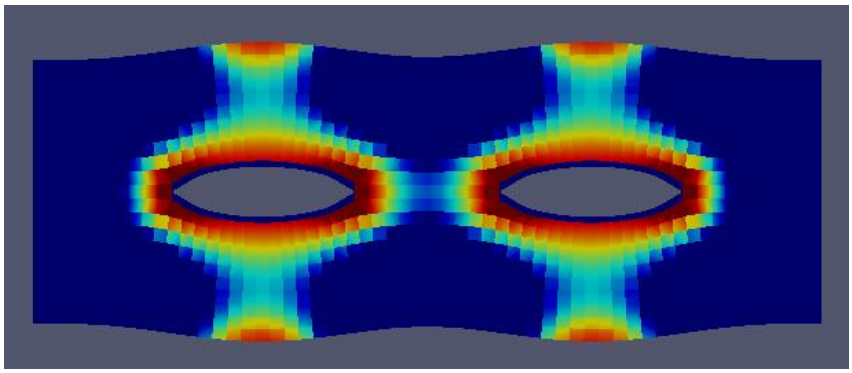

Acknowledgements

First of all, I would like to thank my advisor, Antonio Rodríguez, for his guidance all along the development of this thesis. Antonio, thanks for your patience and advise on the long afternoon meetings, for your motivation and encouragement to work hard and above all, for valuing my effort. Many thanks as well to Elena Tamayo-Mas for sharing her PhD codes and for her initial suggestions to drive this thesis and to Jordi Feliu for his help on Paraview visualisations.

I would also like to express my gratitude to my parents and my brother, who after hearing me talking non-stop about this work, may be already experts in fracture. *Family, gràcies pel suport que m'heu donat aquests anys i per inculcar-me els valors de l'esforç desde petita. No hauria arribat fins aquí sense vosaltres.*

Finally, I would like to thank Jordi for the mutual support during the elaboration of our thesis. I'm really grateful for having found someone to share the ambition of being skilled engineers.

Contents

List of Figures

List of Tables

Chapter 1

Introduction

1.1 Motivation

In engineering there is a wide range of occasions where dealing with material failure is an essential task. Typically, quasi-brittle materials –concrete or rocks, for instance– are studied with one of these two approaches: (a) damage mechanics, where a continuous model is used to analyse the first stages of the failure process, like damage inception and propagation; or (b) fracture mechanics, where a discontinuous model is used to study the last stages of the failure process, treating cracks and material separation, see Sukumar et al. (2015).

Even though continuous models may be accurate enough to model discontinuities, in some specific cases, the explicit representation of the crack is of interest. Then a discontinuous approach may be recommended. Furthermore, this approach can provide a useful technique to study the interaction between the material and a fluid flowing inside a crack. To this end, the discontinuous approach can be used to model the introduction of pressure generated by the fluid.

One of the fields where this technique could be applied is in hydraulic fracturing, see Figure 1.1. This activity involves the injection of a liquid at high pressure with the objective of breaking rocks to obtain oil or gas. The response of the fractured rock and the crack path generated can be modelled with this strategy.

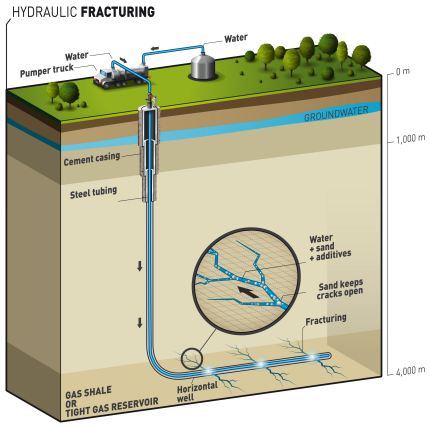

Figure 1.1: Hydraulic fracturing is one of the fields where the proposed model can be applied.

Another possible application is the study of the ground behaviour of roads in poor condition, see Figure 1.2. Water can easily flow inside pre-existing cracks, generating pressure when it freezes in winter. The proposed technique allows to more clearly simulate pavement degradation.

Figure 1.2: Filtrated water freezes and generates pressure in the crack.

One final example of possible applications is carbon sequestration, see Figure 1.3. This activity consists on storing carbon dioxide in underground cavities, preventing it from being emitted to the atmosphere, Herzog (2009). Existing cracks can be analysed in order to guarantee a safe storage of the captured carbon dioxide.

A continuous-discontinuous model proposed by Tamayo-Mas (2013) has been proved to be suitable for dealing with failure of quasi-brittle materials. This thesis presents a new contribution to the work cited, introducing the effect of a fluid pressure, once the crack discontinuity is generated.

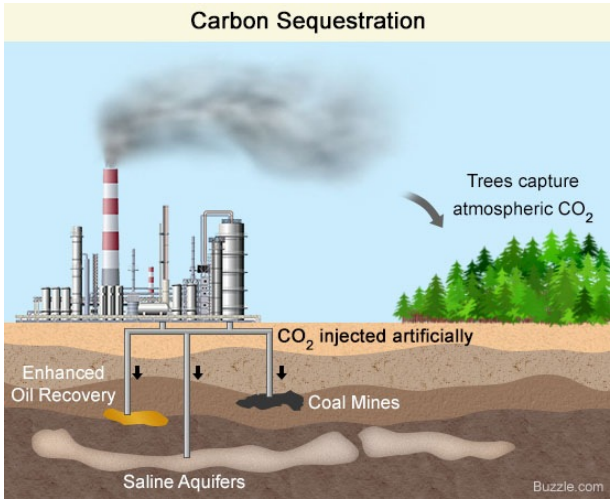

Figure 1.3: Carbon sequestration injects carbon dioxide underground.

1.2 State of the art

Dealing with failure of quasi-brittle materials –such as concrete or rocks– is typically treated following two approaches: damage mechanics and fracture mechanics, corresponding to continuous and discontinuous models, respectively. Regarding the modelling of a crack, continuous models work with a smeared representation of the crack, understood as an area with high strain concentration. Discontinuous models, instead, deal with an explicit representation, provided by the displacement jump.

In this section, both continuous and discontinuous models are discussed. The main difficulties and the techniques arisen to solve them are outlined.

1.2.1 Continuous models

Continuous models tackle the failure phenomena from the point of view of damage mechanics. These approaches consider a continuously differentiable displacement field. Hence, a continuous strain field is derived. Then, fracture is described as a process of strain localisation and damage growth, and cracks are represented by continuum regions that have lost their local load-carrying capacity.

The constitutive laws required for the description of quasi-brittle materials must present strain softening. This means that the stress-strain law is nearly linear up to the peak

stress and decreases after reaching it. Classical continuum theories use local models, that is that the stress at a point only depends on the strain history at that point. When they are used, results exhibit a pathological mesh-dependence, leading to unrealistic results.

In order to overcome this sensitivity to discretisation parameters –such as mesh size– several solutions have been proposed in the literature, Rabczuk (2013).

Crack-band approach

The crack-band model, presented by Bažant and Oh (1983), consists of adjusting the post-peak slope of the stress-strain curve by means of the element size. Nevertheless, as discussed by Jirásek and Bauer (2012), the criterion for estimating the width of the crack band is not straightforward. In fact, it depends on several parameters such as the element type, the element shape and the direction of the crack band with respect to the mesh edges.

Regularised formulations

These models prevent strain localisation into an arbitrarily small volume by means of an additional material parameter: the characteristic length ℓ. However, this internal length parameter cannot be directly measured and it may be only inferred by inverse analysis of test results. These models include non-local integral and gradient-enriched formulations.

In *integral-type* models, an internal variable Y is replaced by its non-local counterpart $\widetilde{Y}$, computed by weighted averaging of Y. For a detailed overview of non-local formulations that provide an appropriate description of the complete failure process, see Bažant and Jirásek (2002).

Gradient-type non-local models, see de Borst et al. (1995) and Peerlings et al. (1998), set a differential –rather than integral– relation between local and non-local variables. Indeed, a partial differential equation (PDE) relating the local and non-local variables is added to the system. Tamayo-Mas (2013) discusses the choice of the appropriate boundary conditions that the PDE requires.

In this dissertation, a gradient-enriched formulation is used to regularise softening. However, the non-locality is introduced at the level of displacements, as presented by Rodríguez-Ferran et al. (2005).

1.2.2 Discontinuous models

Discontinuous models deal with the failure process from the point of view of fracture mechanics. These approaches consider a discontinuous displacement field. Hence, the strain field has, on the one hand, a regular part computed by standard differentiation of the displacement field, and on the other hand, a singular part considering the contributions of the displacement jump. This allows the crack to be represented explicitly.

Several approaches to handle displacement discontinuities have been proposed in the literature and provide a reliable simulation of failure processes, see (Simo et al. (1993), Simo and Oliver (1994) and Armero and Garikipati (1996)). Despite that, standard finite element approximations cannot capture strong discontinuities. Some computational methods are outlined in this section, for a detailed review, see Jirásek and Bauer (2012) and Rabczuk (2013).

Remeshing

In remeshing methods, the standard finite element method (FEM) is used. However, the element edges –in 2D– must be aligned with the crack and the nodes located on these edges must be doubled. Due to this, the finite element mesh must be reconstructed each time the crack propagates.

Embedded discontinuities

As presented by Ortiz et al. (1987) and Belytschko et al. (1988), displacement jumps are captured by enriching the approximation of the displacement field with additional parameters. The need of remeshing when propagation occurs is avoided and reduced changes in finite element codes are required since the enrichment is elemental.

eXtended Finite Element Method (X-FEM)

X-FEM is widely used to simulate the presence of crack in a finite element framework. It is based on the partition of unity concept, which is considered to decompose the displacement field into a continuous and a discontinuous part. That is, the standard finite element (FE) interpolation of the displacement field is enriched with discontinuous functions. The enrichment employed in this technique is nodal.

Approaches of a different nature exist as well. *Meshless methods*, Belytschko et al. (1996) and Nguyen et al. (2008), efficiently model evolving discontinuities because of the absence

of a mesh. In *phase-field methods*, cracks are assumed to propagate along the minimum energy path, see Bourdin et al. (2000) and Francfort and Marigo (1998).

In this thesis, X-FEM is the technique used to introduce the crack discontinuity.

1.2.3 Continuous-discontinuous models

Continuous models are suitable to describe the early stages of the failure process, between the undamaged state and macroscopic crack initiation. Once the crack is introduced, discontinuous models are appropriate to simulate the last stages, incorporating into the model discontinuous displacement fields. Then, a combination of both approaches has arisen to achieve a better description of the entire failure process: the continuous-discontinuous models (see for instance Mazars and Pijaudier-Cabot (1996), Jirásek and Zimmermann (2001), Wells et al. (2002), Simone et al. (2003) and Comi et al. (2007)).

The continuous-discontinuous technique can be summarised in several stages:

1. **Continuous regime.** For the first stages of the failure process, non-local continuous models are used. This permits to study damage inception and propagation.

2. **Transition.** Once the switching criterion is fulfilled, a discontinuity is introduced. In order to develop an appropriate transition, some issues must be examined:

   - **Switching criterion.** The transition from a continuous to a discontinuous model is carried out when the damage field reaches a critical value D_{crit}. This critical value determines whether traction-free cracks are introduced (the material is fully degraded) or cohesive cracks are inserted (otherwise).
   - **Crack path definition.** The crack path cannot be analytically derived because linear elastic fracture mechanics cannot be employed in a regularised bulk. Generally, it is assumed to be known before-hand.
   - **Energy consistency.** When switching from the continuous model to the discontinuous, the energy not yet dissipated by the bulk has to be transferred to the cohesive crack. The computation of this energy is not straightforward and the extension to a multidimensional setting needs further improvements.

3. **Discontinuous regime.** The final stages of the failure process are modelled: explicit macroscopic cracks and material separation.

1.3 Goals and layout of this thesis

The objective of this thesis is to develop a finite element approach to introduce fluid pressure in a crack. To this end, three goals have been conceived:

1. **To propose a technique to consider the action of fluid pressure in a pre-existing crack.** X-FEM has been proved to be efficient when treating with strong discontinuities, see Belytschko and Black (1999) and Moës et al. (1999). In Chapter 2, the enrichment of the continuous displacement field with this technique in order to introduce displacement jumps is discussed. Furthermore, special emphasis is focused on the contribution of the pressure term p in the FE approach and on the computation of nodal forces in a cracked element.

2. **To apply the proposed technique to a crack in an elastic bulk.** In Chapter 3, a continuous elastic model is used to simulate the response of the material. The behaviour of different cracks –considered to be known *a priori*– in a bulk is analysed. At the end of the chapter, crack propagation caused by fluid pressure is studied.

3. **To apply the proposed technique to a crack in a damageable bulk.** In Chapter 4, a continuous damage model is used to simulate the crack behaviour. In this chapter, the problem of pathological mesh dependence must be solved by means of regularised formulation, as discussed by Tamayo-Mas (2013). The Mazars damage model, Mazars (1986), is used to analyse the behaviour of a pre-existing crack in the damageable bulk.

Chapter 2

Introduction of pressure in a crack

The aim of this chapter is to present a technique to introduce pressure in a pre-existing crack using discontinuous displacement fields.

The eXtended Finite Element Method (X-FEM) is employed to reproduce the crack. The discontinuity is inserted by means of a decomposition of the displacement field into a continuous part and a discontinuous part. Hence, the obtained displacement field is

$$\mathbf{u}(\mathbf{x}) = \mathbf{u}^1(\mathbf{x}) + \psi(\mathbf{x})\mathbf{u}^2(\mathbf{x}) \tag{2.1}$$

where $\mathbf{u}^1$ and $\mathbf{u}^2$ are continuous functions and ψ is the sign function centred at the discontinuity and defined as

$$\psi(\mathbf{x}) = \begin{cases} -1 & \text{if} \quad \mathbf{x} \in \Omega^- \\ 1 & \text{if} \quad \mathbf{x} \in \Omega^+ \end{cases} \tag{2.2}$$

An interesting feature of X-FEM is that nodes along the crack are not needed to introduce pressure in the crack. In further sections, this technique is implemented in order to illustrate it.

2.1 One-dimensional particularisation: uniaxial tension test

In this section, a one-dimensional particularisation of the continuous-discontinuous model is described. Particularly, a uniaxial tension test on a bar with a discontinuity in the

centre is analysed, see Figure 2.1.

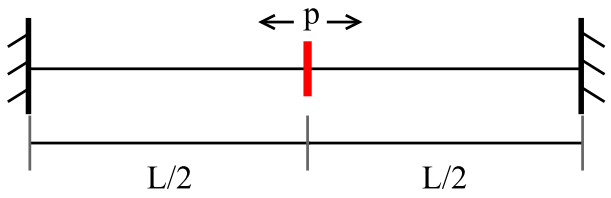

Figure 2.1: Problem statement of the uniaxial tension test.

Governing equations and variational formulation

The equilibrium equation of the problem and its boundary conditions can be summarised as

$$\begin{cases} \sigma'(x) & = & 0 & x \in (0, L) \\ u(0) & = & 0 & \\ u(L) & = & 0 & \\ \sigma(x = L/2) & = & -p & \end{cases} \tag{2.3}$$

where σ is the stress, u is the discontinuous displacement field and p is the pressure introduced in the crack. The displacement field described in Eq. (2.1) can be now defined as $u(x) = u^1(x) + \psi(x)u^2(x)$, where

$$\psi(x) = \begin{cases} -1 & \text{if} \quad 0 < x < \frac{L}{2} \\ 1 & \text{if} \quad \frac{L}{2} < x < L \end{cases} \tag{2.4}$$

It is interesting to remark that there are infinite decompositions of the same displacement field $u(x)$ into $u^1(x)$ and $u^2(x)$. Thus, Dirichlet boundary conditions can be defined as

$$\begin{aligned} u^1(0) &= 0 \qquad & u^2(0) &= 0 \\ u^1(L) &= 0 \qquad & u^2(L) &= 0 \end{aligned} \tag{2.5}$$

The space of admissible displacement variations is decomposed as well by $\omega(x) = \omega^1(x) + \psi(x)\omega^2(x)$, with Dirichlet boundary conditions $\omega^1(0) = \omega^1(L) = \omega^2(0) = \omega^2(L) = 0$ and ψ the sign function defined by Eq. (2.4).

Following the weighted residual method and taking into account the decomposition of the test function $w(x)$, the equilibrium equation is cast in a weak form. Then, following standard procedures, see Appendix A.1 for details, the two variational statements obtained read

$$\int_0^L (\omega^1)'\sigma \, \mathrm{d}x = 0 \tag{2.6a}$$

$$\int_0^L \psi(x)(\omega^2)'\sigma \, \mathrm{d}x = 2\omega^2(L/2)p \tag{2.6b}$$

Since a local elastic model is considered, σ is a function that depends on the strain, ε, where

$$\varepsilon(x) = u'(x) \qquad \Rightarrow \qquad \sigma(x) = E\varepsilon(x) = Eu'(x) \tag{2.7}$$

and E is the Young's modulus.

According to the displacement field decomposition in Eq. (2.1) and the sign function in Eq. (2.4), the stress σ can be defined as

$$\sigma(x) = \begin{cases} E(u^{1'} - u^{2'}) & \text{if} \quad 0 < x < \frac{L}{2} \\ E(u^{1'} + u^{2'}) & \text{if} \quad \frac{L}{2} < x < L \end{cases} \tag{2.8}$$

Finite element discretisation

In order to carry out the calculation, a three-finite element mesh is used. The bar is discretised as described in Figure 2.2.

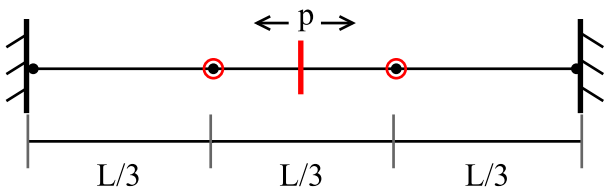

Figure 2.2: Problem discretisation for the uniaxial tension test.

Finite element discretisation of the weak form in Eq. (2.6), see Appendix A.2 for details, leads to the discrete weak forms

$$\int_0^L (\omega^1)'\sigma \mathrm{d}x = 0 \qquad \Rightarrow \qquad \mathbf{K_{a,a}}\,\mathbf{a} + \mathbf{K_{a,b}}\,\mathbf{b} = \mathbf{0} \tag{2.9a}$$

$$\int_0^L \psi(\omega^2)'\sigma \mathrm{d}x = 2\omega^2(L/2)p \qquad \Rightarrow \qquad \mathbf{K_{b,a}}\,\mathbf{a} + \mathbf{K_{b,b}}\,\mathbf{b} = \mathbf{f} \tag{2.9b}$$

where

$$\mathbf{K_{a,a}} = \mathbf{K_{b,b}} := E \int_0^L \mathbf{N}'^T \mathbf{N}' \mathrm{d}x \tag{2.10a}$$

$$\mathbf{K_{a,b}} = \mathbf{K_{b,a}} := E \int_0^L \psi \mathbf{N}'^T \mathbf{N}' \mathrm{d}x \tag{2.10b}$$

$\mathbf{N}^{'}$ is the matrix of shape functions and $\mathbf{a}$ and $\mathbf{b}$ are the vectors of nodal displacements associated to u^1 and u^2 respectively.

It can be observed that the pressure p only appears in the weak form corresponding to the discontinuous test functions, see Eq. (2.9b). This is the expected behaviour because the crack pressure has zero virtual work for continuous virtual displacements.

The stiffness matrix $\mathbf{K}$ can be now assembled as

$$\mathbf{K} = \begin{bmatrix} \mathbf{K_{a,a}} & \mathbf{K_{a,b}} \\ \mathbf{K_{b,a}} & \mathbf{K_{b,b}} \end{bmatrix} \tag{2.11}$$

and the nodal force vector $\mathbf{f}$ reads

$$\mathbf{f} = 2pN_i(L/2) = \begin{pmatrix} 0 & p & p & 0 \end{pmatrix}^T \tag{2.12}$$

Note that only nodes belonging to elements with a discontinuity present the pressure p, that is b_2 and b_3. Indeed, enrichment is only applied to nodes in elements with discontinuity.

The global system of equations $\mathbf{Kx} = \mathbf{f}$ reads

$$\frac{E}{h}\begin{bmatrix} 2 & -1 & -1 & 0 \\ -1 & 2 & 0 & 1 \\ -1 & 0 & 2 & -1 \\ 0 & 1 & -1 & 2 \end{bmatrix}\begin{bmatrix} a_2 \\ a_3 \\ b_2 \\ b_3 \end{bmatrix} = p\begin{bmatrix} 0 \\ 0 \\ 1 \\ 1 \end{bmatrix} \tag{2.13}$$

after setting $a_1 = 0$, $a_4 = 0$, as boundary conditions state; $b_1 = 0$, $b_4 = 0$, since only nodes in elements with a discontinuity are enriched; and h the element size, $h = L/3$.

The solution is

$$\mathbf{x} = \begin{pmatrix} a_2 & a_3 & b_2 & b_3 \end{pmatrix}^T = \frac{p}{E}\begin{pmatrix} \frac{1}{2}h & \frac{-1}{2}h & \frac{3}{2}h & \frac{3}{2}h \end{pmatrix}^T \tag{2.14}$$

It is noted that the displacements obtained are proportional to the mesh size h and a strain defined as p/E.

Considering the displacement decomposition in Eq. (2.1) and the sign function definition in Eq. (2.4), the nodal displacements in the bar are computed and read

$$u_2 = a_2 - b_2 = -h\frac{p}{E} \tag{2.15a}$$

$$u_3 = a_3 + b_3 = h\frac{p}{E} \tag{2.15b}$$

It can be derived from these results that the crack opens following the expected symmetry. It is interesting to determine the crack opening $[|u|]$ in the discontinuity, computing the displacement in the middle section by nodal interpolation:

$$u(L^-/2) = \frac{a_2 + a_3}{2} - \frac{b_2 + b_3}{2} = \frac{-3}{2} h \frac{p}{E} \tag{2.16a}$$

$$u(L^+/2) = \frac{a_2 + a_3}{2} + \frac{b_2 + b_3}{2} = \frac{3}{2} h \frac{p}{E} \tag{2.16b}$$

and

$$[|u|] = u(L^+/2) - u(L^-/2) = 3h\frac{p}{E} = L\frac{p}{E} \tag{2.17}$$

Note that the crack opening can be computed as well as

$$[|u|] = b_2 + b_3 = \frac{3}{2}h + \frac{3}{2}h = 3h\frac{p}{E} = L\frac{p}{E} \tag{2.18}$$

This definition corresponds with the fact that only enriched nodes b_i are used to introduce discontinuities, whereas a_i nodes control continuity. In Figure 2.3 the crack opening computed above can be observed. Note that the jump is indeed $3h\frac{p}{E} = L\frac{p}{E}$.

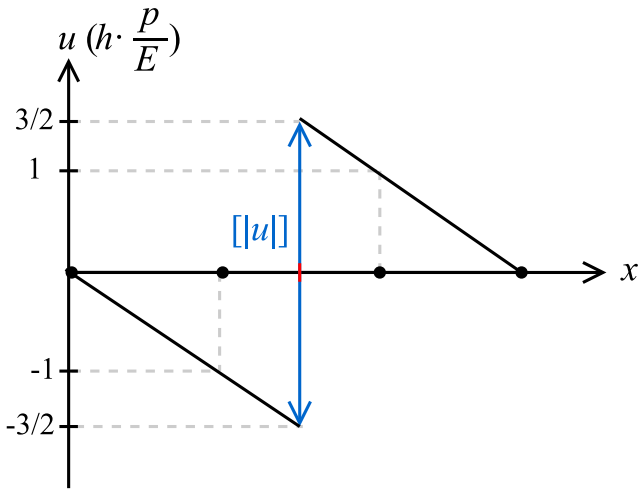

Figure 2.3: Displacement field and crack opening.

2.2 Two-dimensional extension

An extension of the technique to a two-dimensional problem is introduced in this section. In this case, a square element with a vertical crack in the centre is considered, see Figure

2.4.

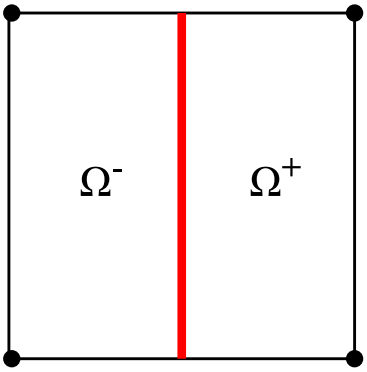

Figure 2.4: 2D element with vertical crack.

Stiffness matrix and rigid modes

An issue of importance in this analysis are the rigid modes of the element. With the purpose of verifying them, the eigenvalues of the cracked element must be computed. To carry this out, the stiffness matrix is needed, see Eq. (2.19) and (2.20),

$$\mathbf{K} = \begin{bmatrix} \mathbf{K_{a,a}} & \mathbf{K_{a,b}} \\ \mathbf{K_{b,a}} & \mathbf{K_{b,b}} \end{bmatrix} \tag{2.19}$$

where

$$\mathbf{K_{a,a}} = \mathbf{K_{b,b}} := \int_{\Omega} \mathbf{B}^T \mathbf{D} \mathbf{B} \, \mathrm{d}\Omega \tag{2.20a}$$

$$\mathbf{K_{a,b}} = \mathbf{K_{b,a}} := \int_{\Omega} \psi \mathbf{B}^T \mathbf{D} \mathbf{B} \, \mathrm{d}\Omega \tag{2.20b}$$

$$= \int_{\Omega^-} \psi \mathbf{B}^T \mathbf{D} \mathbf{B} \, \mathrm{d}\Omega + \int_{\Omega^+} \psi \mathbf{B}^T \mathbf{D} \mathbf{B} \, \mathrm{d}\Omega$$

with $\mathbf{B}$ the matrix of shape functions derivatives and $\mathbf{D}$ the elastic constitutive matrix.

The function *eig* in Matlab computes the eigenvalues of matrix $\mathbf{K}$. The eigenvalue $\lambda = 0$ has a multiplicity of six. This means that the cracked element exhibits six rigid modes, corresponding to a horizontal translation, a vertical translation and an infinitesimal rotation for each part, Ω^- and Ω^+, as depicted in Figure 2.5. Therefore, the crack effectively cuts the element into two fully independent halves.

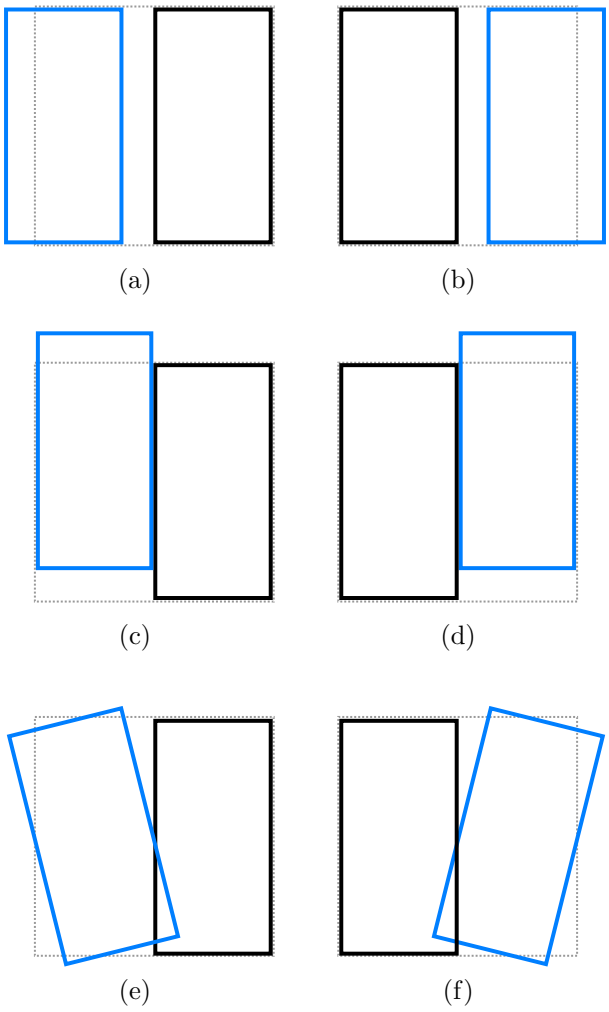

Figure 2.5: Six rigid modes of a quadrilateral cracked element. (a) and (b) are horizontal translations, (c) and (d) vertical translations and (e) and (f) infinitesimal rotations.

Nodal forces

The computation of the nodal force vector $\mathbf{f}$ is now discussed. As mentioned previously, it is not required to have nodes on the crack line. The nodal forces caused by pressure are obtained by calculating line integrals along the crack line.

Following standard procedures, the variational formulation of the problem and its discrete weak form can be determined. Hence, the expression of the nodal force vector can be derived as

$$2\int_{\Gamma_D} p\,\mathbf{v^2 n}\,\mathrm{d}\Gamma = 2p\sum_j \mathbf{v}_j^2 \cdot \int_{\Gamma_D} N_j(\mathbf{x})\cdot\mathbf{n}\,\mathrm{d}\Gamma = \sum_j \mathbf{v}_j^2 \cdot \mathbf{f_j^P} \tag{2.21}$$

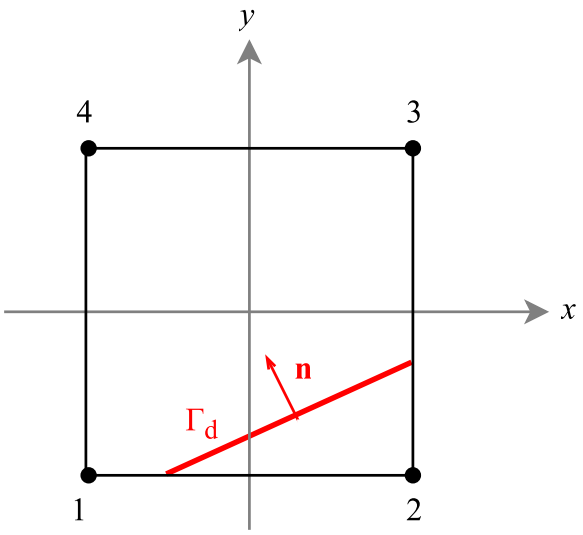

Figure 2.6: Notations for an element with a crack.

Therefore, nodal forces are computed by

$$\mathbf{f} = 2p\, I_j \cdot \mathbf{n}, \tag{2.22}$$

with line integrals defined as

$$I_j = \int_{\Gamma_d} N_j \, \mathrm{d}\Gamma \tag{2.23}$$

where p is the pressure introduced, Γ_d the boundary of the crack, $\mathbf{n}$ the unit normal to Γ_d, see Figure 2.6, and N_j the two-dimensional shape functions defined as

$$N_j(x, y) = \frac{1}{4}(1 \pm x)(1 \pm y) \qquad j = 1, 2, 3, 4 \tag{2.24}$$

It can be easily proved that

$$\sum_j^4 N_j(x, y) = 1 \tag{2.25}$$

From Eq. (2.25) a property regarding the length of the crack can be derived, see Eq. (2.26). Thus, it can be used to validate the computation of line integrals.

$$\sum_j^4 I_j(x, y) = L \tag{2.26}$$

where L is the length of the crack.

Crack opening

The crack opening of a square element with all nodes blocked is now computed, see Fig. 2.7.

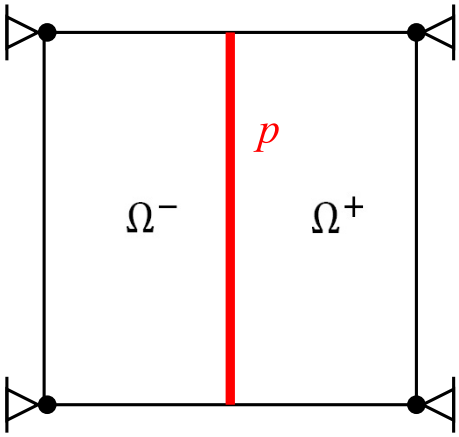

Figure 2.7: Problem statement of a square element with a centred discontinuity.

The boundary conditions are prescribed using Lagrange multipliers:

$$\begin{bmatrix} \mathbf{K} & \mathbf{A}^T \\ \mathbf{A} & \mathbf{0} \end{bmatrix} \begin{bmatrix} \mathbf{u} \\ \boldsymbol{\lambda} \end{bmatrix} = \begin{bmatrix} \mathbf{f} \\ \mathbf{b} \end{bmatrix} \tag{2.27}$$

where $\mathbf{K}$ is the stiffness matrix defined in Eq. (2.19), $\mathbf{A}$ is the matrix of constraints, $\mathbf{u}$ the displacements field, $\boldsymbol{\lambda}$ the vector of Lagrange multipliers, $\mathbf{f}$ the nodal force vector and $\mathbf{b}$ the right-hand side (RHS) vector.

In order to introduce the boundary conditions, matrix $\mathbf{A}$ and the RHS vector $\mathbf{b}$ must be defined. Since all nodes are blocked it can be stated that

$$\begin{cases} \mathbf{u}_1 = \mathbf{a}_1 - \mathbf{b}_1 = 0 \\ \mathbf{u}_2 = \mathbf{a}_2 + \mathbf{b}_2 = 0 \\ \mathbf{u}_3 = \mathbf{a}_3 + \mathbf{b}_3 = 0 \\ \mathbf{u}_4 = \mathbf{a}_4 - \mathbf{b}_4 = 0 \end{cases} \tag{2.28}$$

For the sake of simplicity, matrix $\mathbf{A}$ is decomposed in matrices $\mathbf{A_a}$ and $\mathbf{A_b}$ for the nodal displacements corresponding to vectors $\mathbf{a}$ and $\mathbf{b}$, respectively. Therefore,

$$\mathbf{A_a} = \begin{bmatrix} \mathbf{I} & \mathbf{0} & \mathbf{0} & \mathbf{0} \\ \mathbf{0} & \mathbf{I} & \mathbf{0} & \mathbf{0} \\ \mathbf{0} & \mathbf{0} & \mathbf{I} & \mathbf{0} \\ \mathbf{0} & \mathbf{0} & \mathbf{0} & \mathbf{I} \end{bmatrix} \tag{2.29a}$$

$$\mathbf{A_b} = \begin{bmatrix} -\mathbf{I} & \mathbf{0} & \mathbf{0} & \mathbf{0} \\ \mathbf{0} & \mathbf{I} & \mathbf{0} & \mathbf{0} \\ \mathbf{0} & \mathbf{0} & \mathbf{I} & \mathbf{0} \\ \mathbf{0} & \mathbf{0} & \mathbf{0} & -\mathbf{I} \end{bmatrix} \tag{2.29b}$$

$$\mathbf{b} = \mathbf{0}^T \tag{2.29c}$$

where $\mathbf{I}$ is the identity matrix of size $n = 2$.

As discussed in section 2.1, the vector of nodal forces has zero values in components corresponding to nodal displacements $\mathbf{a}$ and the contribution of the pressure p in the enriched local displacements $\mathbf{b}$. Hence, the nodal force vector can be defined as

$$\mathbf{f} = \begin{bmatrix} \mathbf{0} & \mathbf{f_p} \end{bmatrix}^T \tag{2.30}$$

The results obtained solving the system of equations in (2.27) read:

$$\mathbf{a} = \frac{p}{E} \begin{pmatrix} 1 & 0 & -1 & 0 & -1 & 0 & 1 & 0 \end{pmatrix}^T \tag{2.31a}$$

$$\mathbf{b} = \frac{p}{E} \begin{pmatrix} 1 & 0 & 1 & 0 & 1 & 0 & 1 & 0 \end{pmatrix}^T \tag{2.31b}$$

Indeed, considering the displacement field decomposition in Eq. (2.1) and the sign function in Eq. (2.2), it can be observed that the displacements in the blocked nodes are zero. Moreover, the vector of Lagrange multipliers $\boldsymbol{\lambda}$ has non-zero values in the x direction, which is the expected result since the constriction of blocking the nodes has to be compensated by reaction forces.

Finally, the crack opening is computed taking into account the definition in Eq. (2.17) or (2.18). It is constant along the crack line and has a value of $2p/E$, see Figure 2.8.

$$[|u_{x,A}|] = b_1 + b_2 = 2\frac{p}{E} \tag{2.32a}$$

$$[|u_{x,B}|] = b_4 + b_3 = 2\frac{p}{E} \tag{2.32b}$$

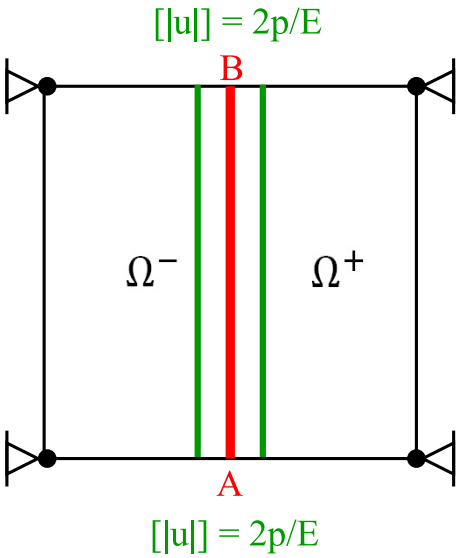

Figure 2.8: Crack opening.

Chapter 3

Discontinuous model of failure for an elastic bulk

3.1 Crack opening in an elastic bulk

Considering the results obtained in Chapter 2 and the technique used to introduce pressure in a pre-existing crack, this section aims to study the crack opening in an elastic bulk. Hence, the Cauchy stress tensor is defined as

$$\boldsymbol{\sigma}(\mathbf{x}) = \mathbf{C} : \boldsymbol{\varepsilon}(\mathbf{x}) = \mathbf{C} : \nabla^s \mathbf{u}(\mathbf{x}) \tag{3.1}$$

where $\mathbf{C}$ is the tensor of elastic moduli, $\boldsymbol{\varepsilon}$ the small strain tensor and ∇^s the symmetrised gradient.

A two-finite element mesh is used assembling elemental stiffness matrices $\mathbf{K}^e$ defined in Eq. (2.19) and obtaining the nodal force vector $\mathbf{f}$ via the computation of line integrals, Eq. (2.22). Several boundary conditions are tested in order to analyse the crack behaviour. Note that as all the elements have a discontinuity, all nodes must be enriched, see Figure 3.1.

All nodes blocked

In the first place, all nodes are blocked, see Figure 3.2(a). Thus, the boundary conditions are prescribed as

$$\mathbf{u}_i = \mathbf{a}_i + \psi \mathbf{b}_i = 0 \qquad i = 1, ..., 6 \tag{3.2}$$

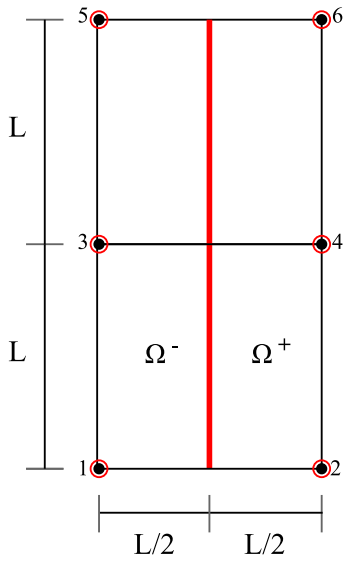

Figure 3.1: Two-finite element mesh with centred crack.

where ψ is the sign function defined in (2.2).

Using the Lagrange multipliers method to prescribe these boundary conditions and considering the displacement decomposition in Eq. (2.1), the crack opening is computed. As expected, a uniform crack opening can be observed along the crack line in Figure 3.2(b).

Corner nodes blocked

A second computation is carried out. In this case, the central nodes, 3 and 4, are not blocked, see Figure 3.3(a). Therefore, only the displacement in nodes 1, 2, 5, 6 must be equal to zero:

$$\mathbf{u}_i = \mathbf{a}_i + \psi \mathbf{b}_i = 0 \qquad i = 1, 2, 5, 6 \tag{3.3}$$

The results are shown in Figure 3.3(b). The crack opening is bigger in this case, where less nodes are blocked. Moreover, it is wider in nodes 3 and 4, where no resistance is applied. It can be observed as well that nodes 3 and 4 move according to the direction of the pressure applied:

$$\mathbf{u}_3 = \mathbf{a}_3 - \mathbf{b}_3 = (-0.3 - 9.0, 0)\frac{p}{E} = (-9.3, 0)\frac{p}{E} \tag{3.4a}$$

$$\mathbf{u}_4 = \mathbf{a}_4 + \mathbf{b}_4 = (0.3 + 9.0, 0)\frac{p}{E} = (9.3, 0)\frac{p}{E} \tag{3.4b}$$

Prescribed displacement

Finally, an inward displacement is prescribed in the central nodes, see Figure 3.4(a).

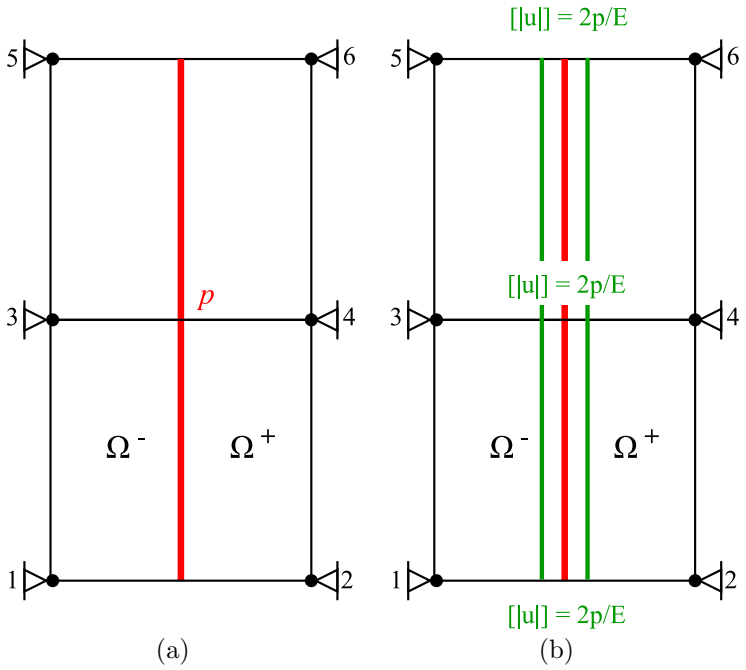

Figure 3.2: All nodes blocked in elastic bulk. (a) Problem statement. (b) Displacement field and crack opening.

Therefore, the RHS vector will have non-zero values in the components corresponding to nodes 3 and 4. To sum up, the boundary conditions can be defined as

$$\mathbf{u}_1 = \mathbf{a}_1 - \mathbf{b}_1 = 0 \tag{3.5a}$$

$$\mathbf{u}_2 = \mathbf{a}_2 + \mathbf{b}_2 = 0 \tag{3.5b}$$

$$\mathbf{u}_3 = \mathbf{a}_3 - \mathbf{b}_3 = \mathbf{u}^* \tag{3.5c}$$

$$\mathbf{u}_4 = \mathbf{a}_4 + \mathbf{b}_4 = -\mathbf{u}^* \tag{3.5d}$$

$$\mathbf{u}_5 = \mathbf{a}_5 - \mathbf{b}_5 = 0 \tag{3.5e}$$

$$\mathbf{u}_6 = \mathbf{a}_6 + \mathbf{b}_6 = 0 \tag{3.5f}$$

In order to carry out a numerical computation, a value of $0.5p/E$ is given to the prescribed displacement $\mathbf{u}^*$. The results can be observed in Figure 3.4(b), where the crack opening is narrower in the central nodes than in the extreme ones, due to $\mathbf{u}^*$.

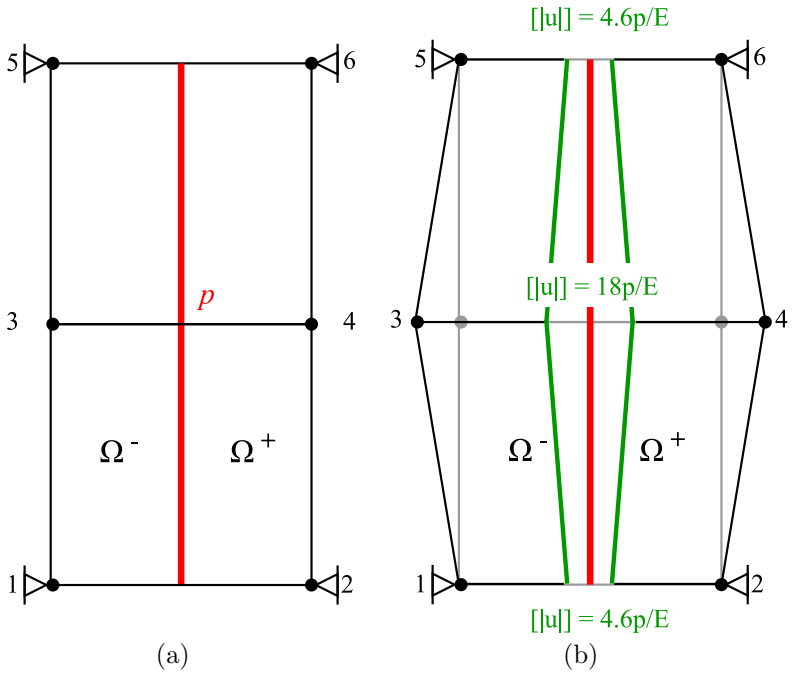

Figure 3.3: Corner nodes blocked in elastic bulk. (a) Problem statement. (b) Displacement field and crack opening.

3.2 Behaviour of a crack in a finite element mesh

Up to now, meshes with only two finite elements have been used. This is useful to illustrate the assembly of elements taking into account the enrichment of the displacement field or the computation of nodal forces corresponding to the pressure applied in the crack. Nevertheless, in numerical problems larger meshes are required.

It is convenient to introduce now the three different types of element taking part in the generation of a finite element mesh containing a crack:

- **Standard element.** Element that is not crossed by any discontinuity and none of its nodes is enriched.
- **Cracked element.** Element that is crossed by a discontinuity and has all or some of its nodes enriched. If the edge of the cracked element contains the crack tip, the nodes belonging to this edge are not enriched. This enrichment criterion is depicted in Figure 3.5.
- **Blending element.** Element that is not crossed by a discontinuity but has some

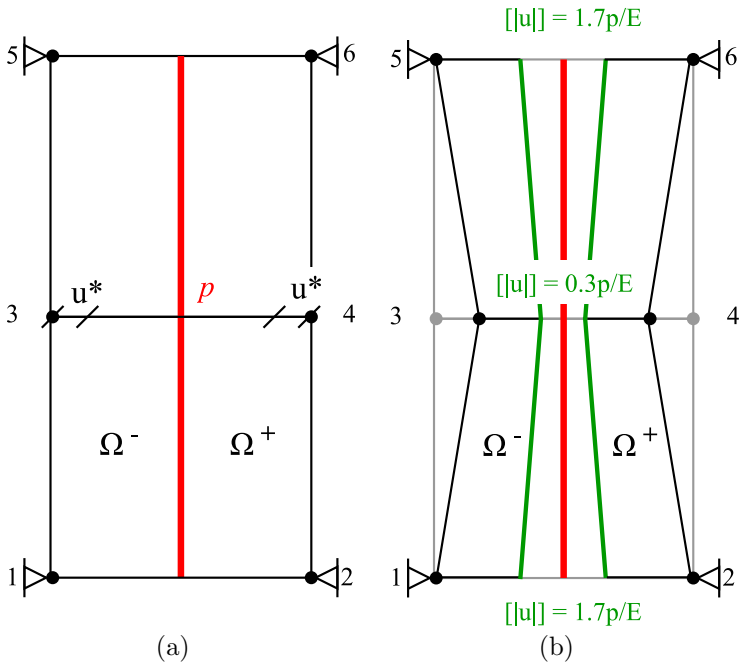

Figure 3.4: Prescribed displacement in elastic bulk. (a) Problem statement. (b) Displacement field and crack opening.

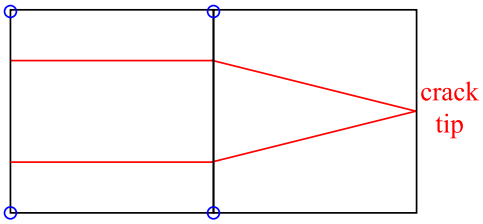

Figure 3.5: Nodal enrichment of a cracked element.

of its nodes enriched– the nodes shared with a cracked element.

These definitions are depicted in Figure 3.6.

Once the treatment of each element is clarified, four examples are shown in order to study the behaviour of a crack in an elastic bulk using a larger mesh. That is an outer crack, an inner crack, two horizontal inner cracks and three inner cracks with different slopes, respectively.

Outer crack

A first test with an outer crack is carried out. In this case, there is only one crack tip. The

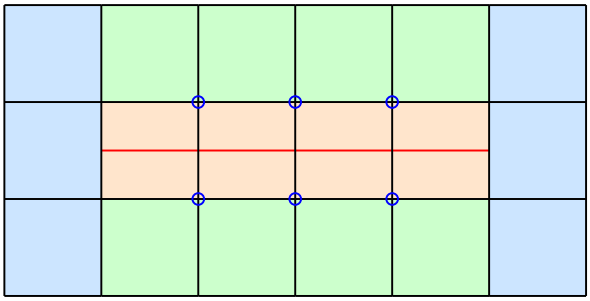

Figure 3.6: Finite element mesh where the different types of element are defined. In blue, standard elements; in orange, cracked elements; in green, blending elements. Enriched nodes are circled.

discontinuity, the nodal enrichment and the mechanical boundary conditions are depicted in Figure 3.7. Square finite elements are used.

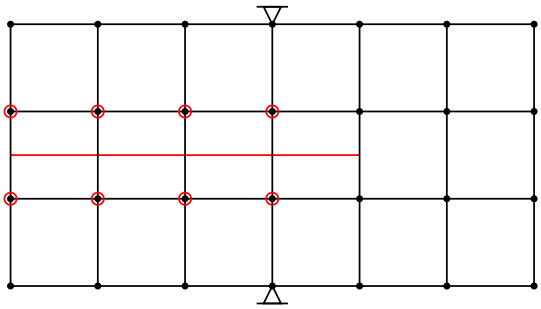

Figure 3.7: Outer crack: problem statement.

Obtaining the nodal force vector $\mathbf{f}$ by the computation of line integrals along the crack and using the Lagrange multipliers method to apply the boundary conditions, the nodal displacements are obtained. As expected, the crack opens and the two separated parts of the bulk bend, see Figure 3.8(b). The crack opening is computed by nodal interpolation, as in Eq. (2.18).

Inner crack

A second test is carried out with a crack originated inside the elastic bulk. In this case, two crack tips appear. The discontinuity, the nodal enrichment and the mechanical boundary conditions are depicted in Figure 3.9.

Following the same procedure as in the outer crack example, the nodal displacements and

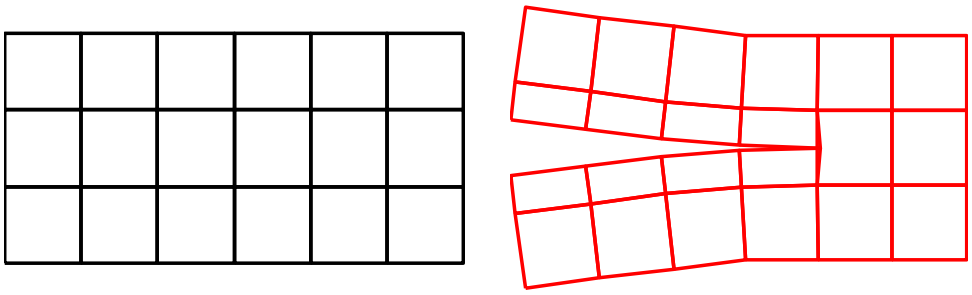

(a) (b)

Figure 3.8: Outer crack: in (a) original mesh, in (b) deformed mesh and crack opening.

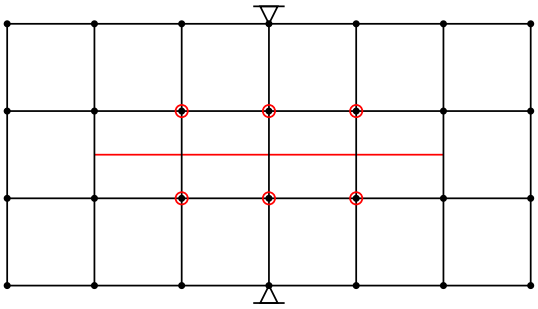

Figure 3.9: Inner crack: problem statement.

the crack opening are computed. The results in Figure 3.10(b) exhibit the expected symmetry and the awaited strain. In addition, it can be observed that the jump displacement in the crack tips is zero.

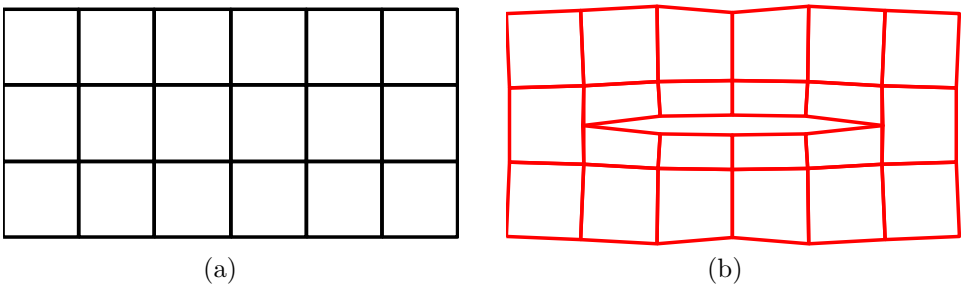

(a) (b)

Figure 3.10: Inner crack: in (a) original mesh, in (b) deformed mesh and crack opening.

Two inner cracks

Now, it is interesting to verify the implementation of the technique in an elastic bulk where two cracks coexist. The mechanical boundary conditions are depicted in Figure

3.11.

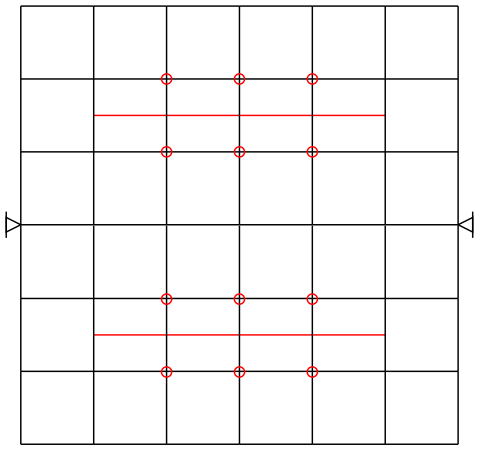

Figure 3.11: Two inner cracks: problem statement.

The nodal displacements and the crack opening shown in Figure 3.12(b) are effectively consistent. Two symmetric cracks are obtained, the displacement jump in the crack tips is zero, the crack opening is wider in the central part of the crack and the bulk exhibits the expected strain.

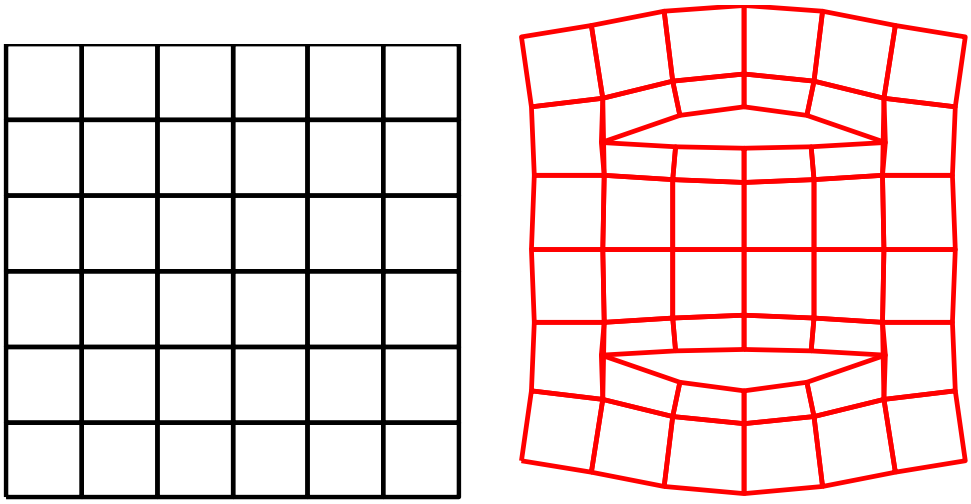

(a) (b)

Figure 3.12: Two inner cracks: in (a) original mesh, in (b) deformed mesh and crack opening.

Three inner cracks with different alignment

Up to now, all the cracks have been aligned to the meshes' edges. In this test, three different cracks, with different slopes are considered, see Figure 3.13. The objective of

this is to validate the application of the method to cracks that are not aligned with the mesh.

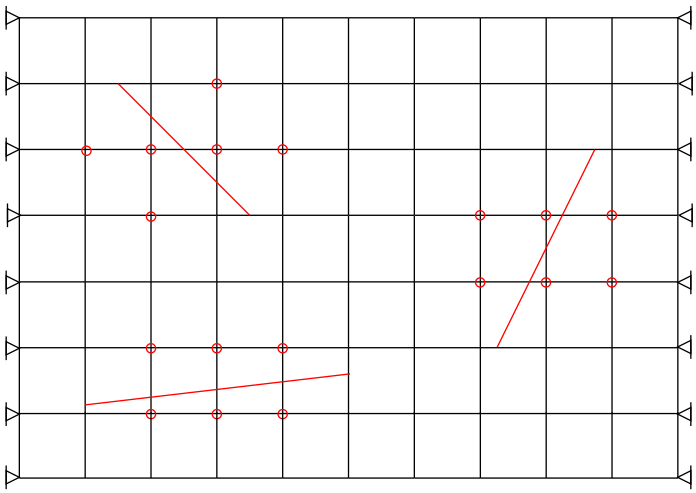

Figure 3.13: Three cracks with different alignment: problem statement.

Following the same procedure as in the previous examples, the displacement field is obtained. Figure 3.14 represents the new mesh coordinates and shows the crack opening of each crack. The expected strain of the bulk is exhibited and crack tips do not have displacement jump. Hence, it can be stated that the proposed technique allows crack location to be independent of the finite element mesh.

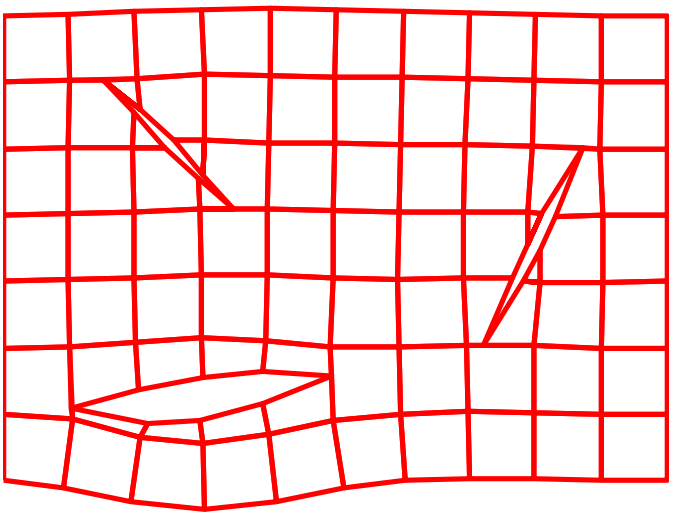

Figure 3.14: Three cracks with different alignment: deformed mesh and crack opening.

3.3 Crack propagation

In this section, the propagation of the crack path is discussed. To do so, an elastic bulk with a pre-existing crack that crosses three finite elements is considered, see Figure 3.15(a). Regarding the boundary conditions, the degrees of freedom of the left and right edges of the bulk are blocked.

The action of the pressure is applied and the nodal displacements and the crack opening are computed using the procedure presented previously, see Figure 3.15(b). After that, the crack is assumed to propagate a distance of one element for each end. Thus, the crack crosses now five finite elements. A transitional state is considered: the crack line increases but the pressure remains as in the previous step, see Figure 3.15(c). Finally, the force vector is updated and the crack opening becomes wider, see Figure 3.15(d). This process can be repeated to continue propagating.

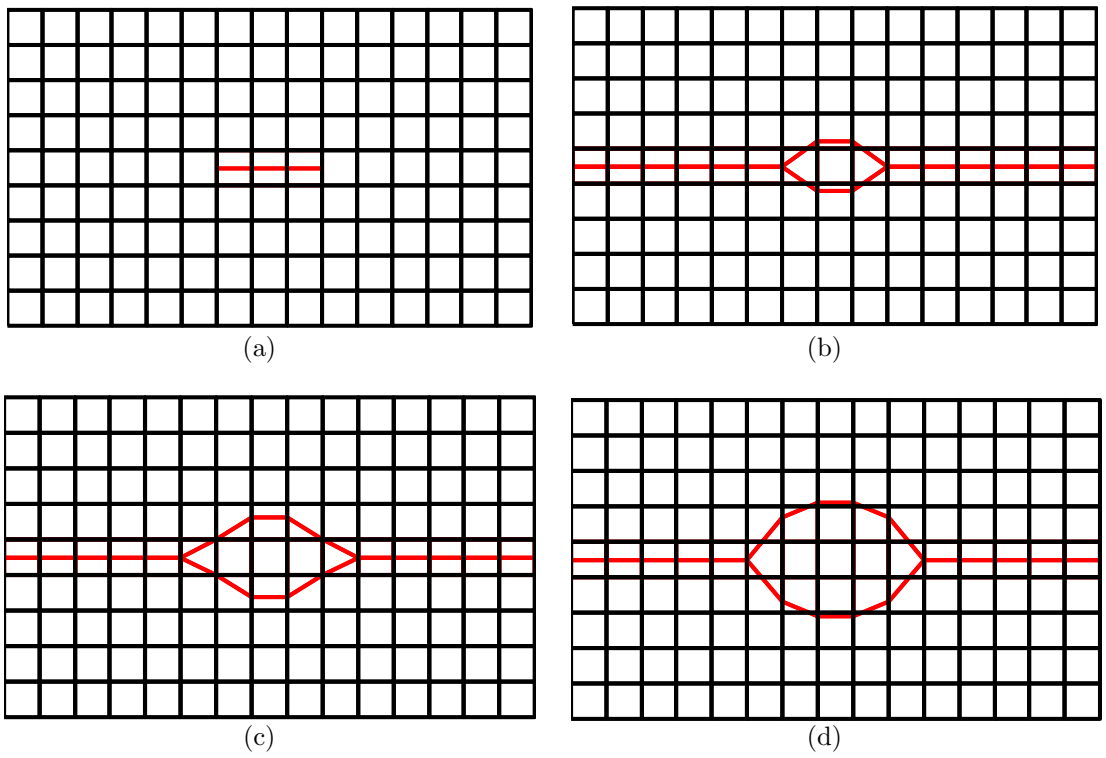

Figure 3.15: Crack propagation. (a) shows the initial crack, (b) the crack opening once the pressure is introduced, in (c) the crack propagates and (d) shows the crack opening caused by the new pressure.

The crack opening due to propagation exhibits the expected response. The crack path can be efficiently determined by means of the simplified medial-axis method (θ-SMA), as discussed by Tamayo-Mas and Rodríguez-Ferran (2015).

Chapter 4

Continuous-discontinuous model of failure for a damageable bulk

In this chapter, a damageable bulk is analysed. The elastic behaviour in Chapter 3 yields a linear problem, whereas in this section a non-linear problem must be solved. The technique used to solve it is the Newton-Raphson method, see Belytschko et al. (2000) and Crisfield (1991).

In Section 4.1 the need for a regularisation is discussed, in Section 4.2 the damage model is presented and finally in Section 4.3, three numerical examples are analysed.

4.1 Regularisation

Gradient-enhanced model based on smoothed displacements

Classical continuum theories typically exhibit pathological mesh-dependence, which provides physically unrealistic results. This means that the element size determines the response. In order to avoid this behaviour, non-locality is introduced at the level of displacements, see Rodríguez-Ferran et al. (2005),

$$\widetilde{\mathbf{u}}\left(\mathbf{x},t\right)-\ell_c^2\nabla^2\widetilde{\mathbf{u}}\left(\mathbf{x},t\right)=\mathbf{u}\left(\mathbf{x},t\right) \tag{4.1}$$

where $\widetilde{\mathbf{u}}$ are the non-local or smoothed displacements, $\mathbf{u}$ the local displacements and ℓ_c the characteristic length of the non-local damage model.

This model computes the non-local displacements $\widetilde{\mathbf{u}}$ from the local displacements $\mathbf{u}$ as the solution of the second-order PDE in Eq. (4.1). Indeed, the regularisation PDE is in this case a diffusion-reaction equation.

Boundary conditions

Appropriate boundary conditions for the smoothed displacement field $\widetilde{\mathbf{u}}$ must be imposed. As discussed in Tamayo-Mas (2013), the combined boundary conditions

$$\left.\begin{array}{rcl} \widetilde{\mathbf{u}}\cdot\mathbf{n} & = & \mathbf{u}\cdot\mathbf{n} \\ \nabla\left(\widetilde{\mathbf{u}}\cdot\mathbf{t}\right)\cdot\mathbf{n} & = & \nabla\left(\mathbf{u}\cdot\mathbf{t}\right)\cdot\mathbf{n} \end{array}\right\} \text{on } \partial\Omega \tag{4.2}$$

where $\mathbf{n}$ denotes the unit normal to Ω and $\mathbf{t}$ is the tangent vector such that $\{\mathbf{n},\mathbf{t}\}$ form an orthonormal basis for $\mathbb{R}^2$; provide the required properties for the regularisation equation.

With this, Dirichlet boundary conditions are prescribed for the normal component of the displacement field and non-homogeneous Neumann boundary conditions are imposed for the tangential components. They are prescribed using the Lagrange multipliers method. In Appendix B, the treatment of the mechanical and the regularisation boundary conditions is discussed.

4.2 Damage model

The damage model used is the simplified Mazars model, which considers only positive strains,

$$Y = \sqrt{\sum_i \left[\max\left(0,\varepsilon_i\right)^2\right]} \tag{4.3}$$

where Y is the local state variable and ε_i are the principal strains.

A linear damage evolution law is considered

$$D(Y) = \frac{Y_f}{Y_f - Y_0}\left(1 - \frac{Y_0}{Y}\right) \tag{4.4}$$

where Y_0 is the damage initiation state variable and Y_f the maximum admissible value for the state variable.

Figure 4.1 shows the linear damage evolution law. The material has an elastic behaviour until it reaches the peak stress, associated to a strain Y_0. This means the beginning

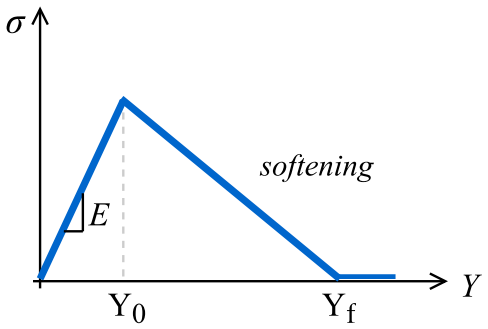

Figure 4.1: Constitutive stress-strain law for the local model.

of the softening. In the second branch, the stiffness of the bulk is reduced. It is an unloading phase until Y_f is reached. Then, the material is fully degraded and the damage parameter D is the maximum, $D = 1$. Even though Figure 4.1 represents the constitutive stress-strain law for the local model, the same idea can be extended to non-local models:

$$\boldsymbol{\sigma}(\boldsymbol{\varepsilon}, \widetilde{\boldsymbol{\varepsilon}}) = [1 - D(\widetilde{\boldsymbol{\varepsilon}})]\, \mathbf{C} : \boldsymbol{\varepsilon} \tag{4.5}$$

4.3 Numerical examples

In this section, three numerical examples are described in order to validate the technique used to introduce pressure in a pre-existing crack, considering a continuous-discontinuous damage model.

First, two tests of a bulk with an inner crack are carried out, refining the finite element mesh. Then, a longer crack line is analysed. Finally, the extension of the model to two cracks in a damageable bulk is discussed.

Finite element mesh refinement

Two tests are carried out using the same damageable bulk. Pressure is introduced in a centred horizontal crack, and the mechanical boundary conditions consist on blocking the degrees of freedom of the lateral edges, see Figure 4.2. The dimensionless geometric and material parameters are summarised in Table 4.1.

Both the mechanical and the regularisation boundary conditions described in Figure 4.2 and Eq. (4.2), respectively, are prescribed using the Lagrange multipliers method, see

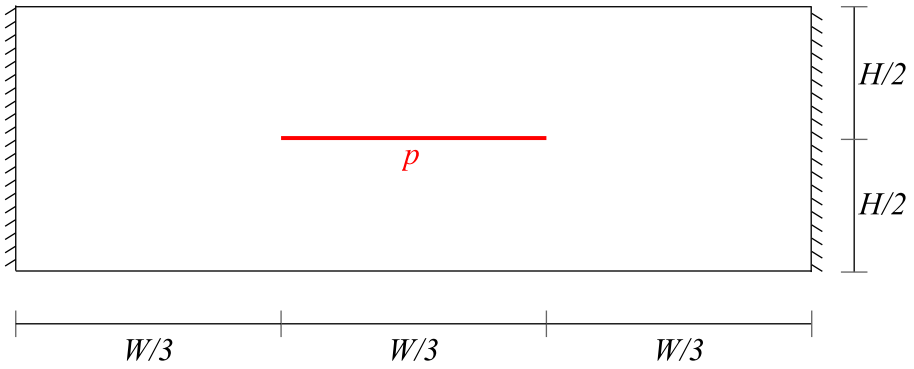

Figure 4.2: Problem statement of a damageable bulk with one inner crack.

Meaning	Symbol	Value
Height of the bulk	H	10
Width of the bulk	W	30
Length of the crack	L_c	10
Young's modulus	E	20 000
Damage threshold	Y_0	10^{-4}
Final strain	Y_f	1.25×10^{-2}

Table 4.1: Inner crack in a damageable bulk: geometric and material parameters.

Appendix B for details.

In the first test, a mesh of 11×30 finite elements is used; whereas in the second one, the discretisation of the problem is performed using a mesh of 21×60 finite elements. Figure 4.3 shows the results of the damage field obtained after having applied the pressure p.

It can be observed that the material breaks following the direction orthogonal to the crack line. In addition, strain can be noticed in the top and bottom edges of the bulk. Besides, the results exhibit the expected symmetry with respect to a horizontal axis. Refining the mesh, more accuracy is obtained in the damage field and a better gradation of it can be observed in Figure 4.3(b), where the mesh is finer.

Figures 4.4(a) and 4.4(b) show the curve pressure-crack opening displacement (COD). Being a damageable bulk, the stiffness of the material, which corresponds to the curve's slope, decreases. Note that in the case of an elastic behaviour, it remains constant.

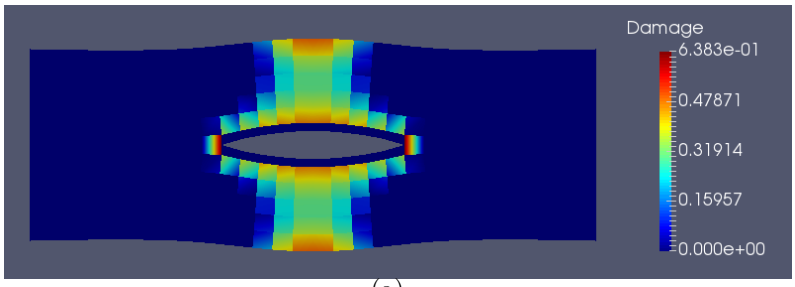

(a)

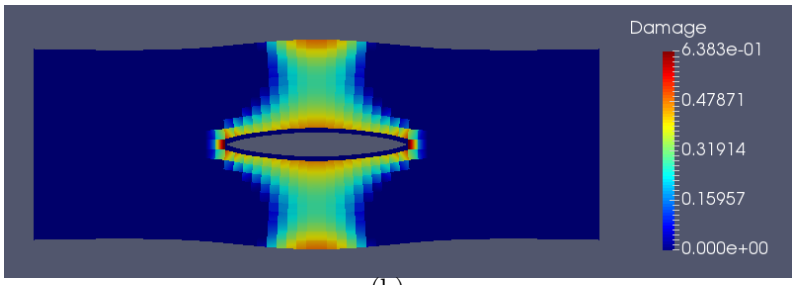

(b)

Figure 4.3: Damage field for a bulk with a centred crack. In (a) a mesh of 11×30 finite elements is used; in (b) a mesh of 21×60 finite elements.

Longer crack

The previous two tests are repeated changing the length of the discontinuity: it is a centred horizontal crack of length $L_c = 2W/3$. The dimensionless geometric and material parameters are summarised in Table 4.2. The same procedure as in the previous example is employed to prescribe the boundary conditions and the same two meshes are used to discretise the problem.

Meaning	Symbol	Value
Height of the bulk	H	10
Width of the bulk	W	30
Length of the crack	L_c	20
Young's modulus	E	20 000
Damage threshold	Y_0	10^{-4}
Final strain	Y_f	1.25×10^{-2}

Table 4.2: Inner longer crack in a damageable bulk: geometric and material parameters.

The damage field is shown in Figure 4.5. As expected, having a longer crack, the bulk is more damaged and it has a higher strain. The expected symmetry is also exhibited.

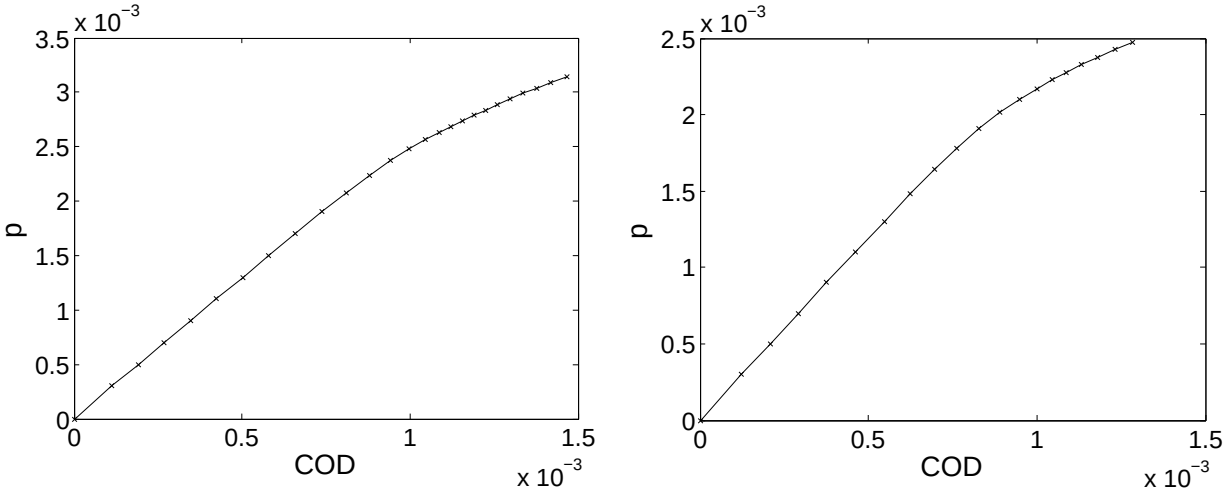

Figure 4.4: Pressure-crack opening displacement (COD). In (a) a mesh of 11×30 finite elements is used; in (b) a mesh of 21×60 finite elements.

Again, the finer mesh shows a better gradation of the damage field and provides more accuracy in the results.

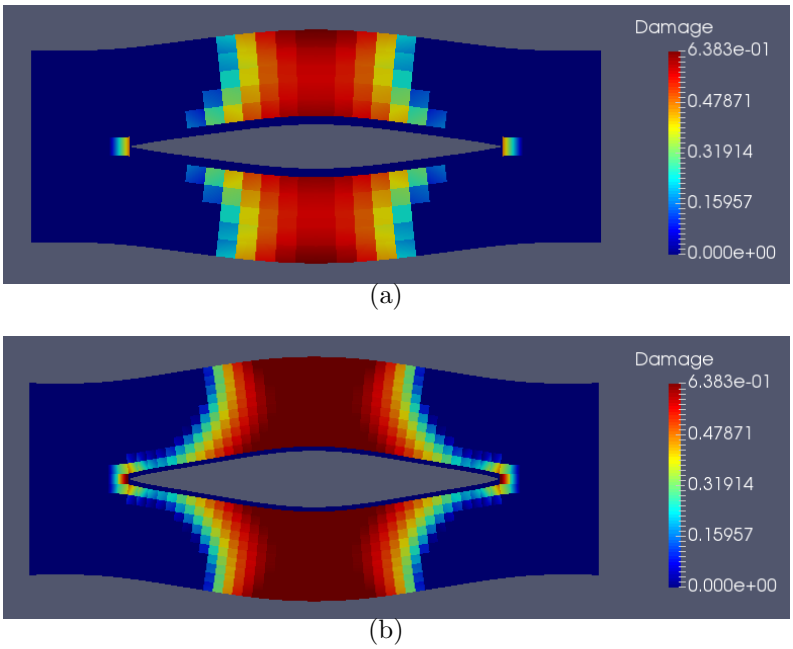

Figure 4.5: Damage field for a bulk with a longer centred crack. In (a) a mesh of 11×30 finite elements is used; in (b) a mesh of 21×60 finite elements.

The curves pressure-COD are presented in Figure 4.6. The loss of the material stiffness is derived from the decrease of the curve's slope in both tests, due to the damageable

behaviour of the bulk.

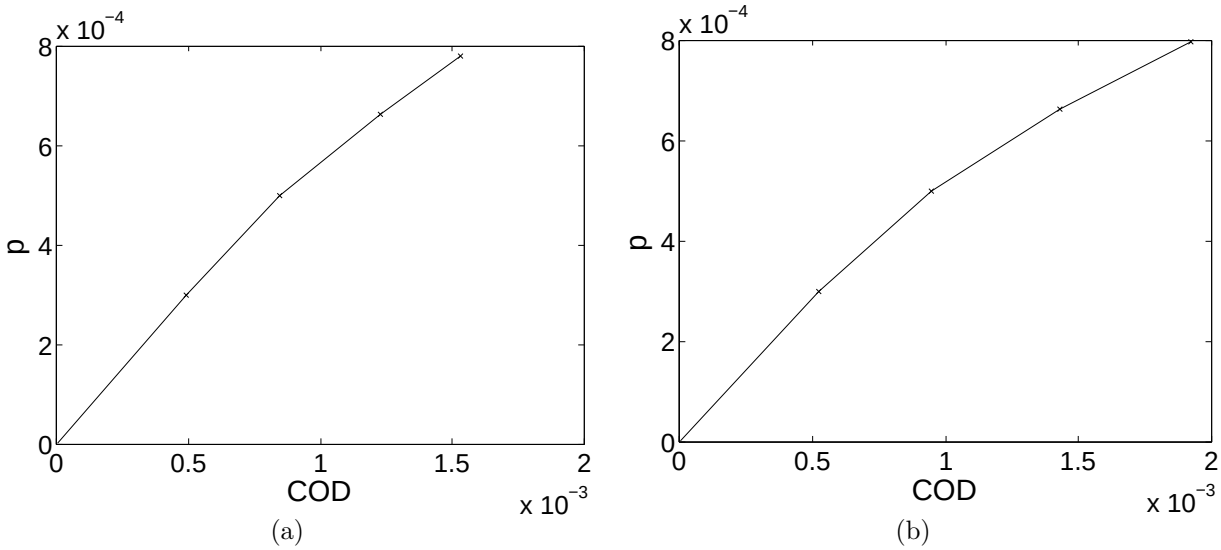

Figure 4.6: Pressure-crack opening displacement (COD). In (a) a mesh of 11×30 finite elements is used; in (b) a mesh of 21×60 finite elements.

Bulk with two cracks

Finally, a damageable bulk with two inner cracks is studied. The problem statement is depicted in Figure 4.7 and the dimensionless geometric and material parameters are described in Table 4.3. The same mechanical and regularisation boundary conditions as in the previous examples are prescribed and again, the Lagrange multipliers method is used to impose them.

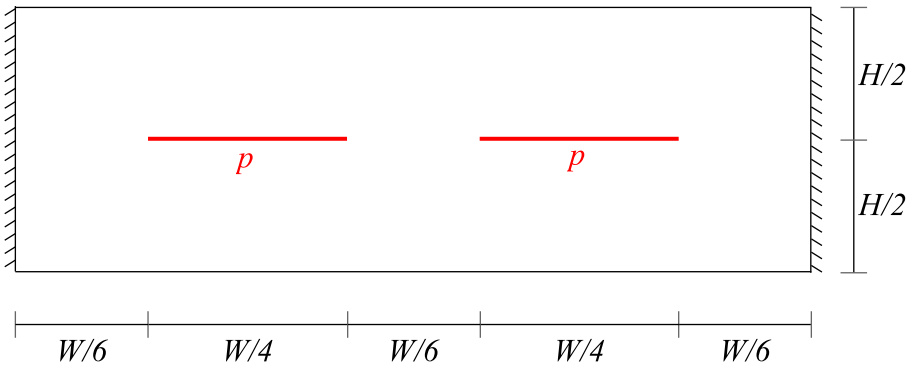

Figure 4.7: Problem statement of a damageable bulk with two inner cracks.

Regarding the discretisation of the problem, a mesh of 21×60 finite elements is employed, since it has been remarked that more accurate results are obtained.

Meaning	Symbol	Value
Height of the bulk	H	10
Width of the bulk	W	30
Length of the crack	L_c	7.5
Young's modulus	E	20 000
Damage threshold	Y_0	10^{-4}
Final strain	Y_f	1.25×10^{-2}

Table 4.3: Two inner cracks in a damageable bulk: geometric and material parameters.

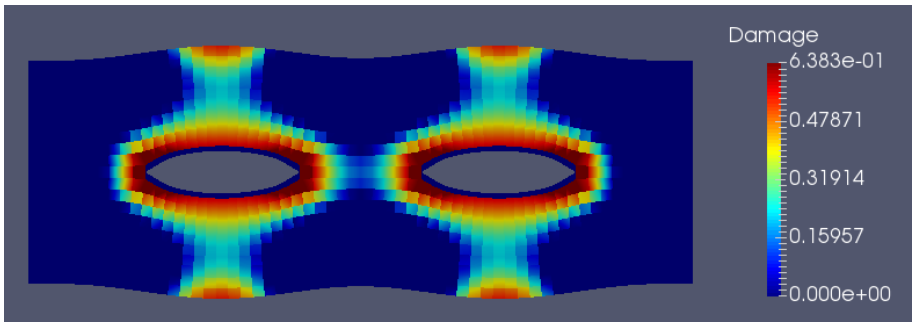

Figure 4.8: Damage field for a bulk with two inner cracks.

The results are shown in Figure 4.8. As presumed, the two cracks produce a symmetrical damage field. Again, the material is damaged following the perpendicular direction to the crack line and its top and bottom edges exhibit the expected strain.

Finally, the curve pressure-COD in Figure 4.9 shows the loss of stiffness, according to the characteristic response of a damageable material.

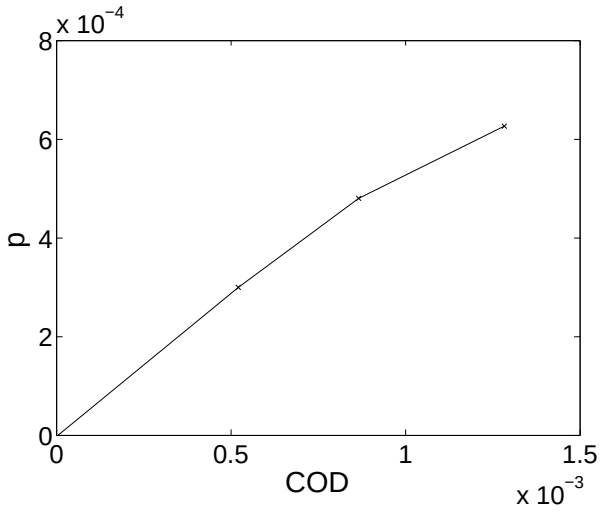

Figure 4.9: Pressure-crack opening displacement (COD).

Chapter 5

Concluding remarks and future work

5.1 Concluding remarks

In this dissertation a finite element approach to introduce fluid pressure in a crack has been developed. To this end, three main contributions discussed in detail in the previous chapters are presented:

1. **A technique to consider the action of fluid pressure in a pre-existing crack has been proposed.** A procedure to treat the pressure term p with X-FEM is presented in Chapter 2. First, the nodal enrichment of the cracked elements has been discussed. Then, the computation of line integrals over the crack line is proved to be an efficient way to obtain nodal forces. Therefore, it can be stated that there is no need to have nodes along the crack in order to consider the pressure applied in it.

2. **The proposed technique has been applied to a crack in an elastic bulk.** In Chapter 3, the crack opening of pre-existing cracks has been computed for an elastic material. The appropriate application of the enriching criteria yields realistic responses of the crack opening. The model has been validated for a bulk with two coexisting cracks and it has been proved that crack locations are completely independent of the finite element mesh. Moreover, the propagation of the crack, element by element, has been properly modelled.

3. **The proposed technique has been applied to a crack in a damageable bulk.** Regularisation has been introduced at the level of displacements, as proposed by Rodríguez-Ferran et al. (2005), in order to avoid pathological mesh-dependence. Consistent damage fields have been obtained for several cracks in Chapter 4. In addition, loss of material stiffness can be observed due to the caused damage. Hence, the model provides a good simulation of failure caused by pressure acting in a pre-existing crack.

5.2 Future work

The work carried out in this dissertation leaves several directions to be discussed in the near future. These open research lines can be summarised as

- **Arc-length or displacement control implementation.** In this work, the force-displacement response is computed using force control. Therefore, the unload branch cannot be obtained. In order to overcome this problem, a displacement control (particularly, a crack opening displacement control) or an arc-length control, see Belytschko et al. (2000) and Crisfield (1991), are recommended.

- **Propagation of crack.** An interesting aspect of the behaviour of the crack is its propagation due to the effect of the pressure. An element-by-element propagation has been developed for the elastic problem. Thus, it would be interesting to extend it to the damageable material. Furthermore, a geometrical crack tracking could be employed by means of the $\theta-$SMA, simplified medial axis, discussed by Tamayo-Mas and Rodríguez-Ferran (2015).

- **Crack inception.** In this work, only pre-existing cracks have been analysed. The whole failure process could be simulated, combining the model presented by Tamayo-Mas (2013), where the crack is generated by external forces with the model presented in this thesis, where crack pressure opens a pre-existing crack.

Appendix A

Variational formulation and discretisation

In this appendix the variational formulation and the discretisation of the one-dimensional problem are described. In Section A.1, the variational formulation of the equilibrium equation is cast in a weak form. Then, in Section A.2, the stiffness matrix is computed.

Special emphasis is placed on the treatment of the discontinuity introduction and the role of pressure acting in the crack.

A.1 Variational formulation

The equilibrium equation and its boundary conditions

$$\begin{cases} \sigma'(x) & = & 0 & \qquad x \in (0, L) \\ u(0) & = & 0 & \\ u(L) & = & 0 & \\ \sigma(x = L/2) & = & -p & \end{cases} \tag{A.1.1}$$

where σ is the stress, u is the discontinuous displacement field and p is the pressure introduced in the crack, are cast in a weak form.

Both the displacement field u and the virtual displacement field ω can be decomposed

into two other continuous displacement fields u^1 and u^2, and ω^1 and ω^2, respectively:

$$u(x) = u^1(x) + \psi(x)u^2(x) \tag{A.1.2a}$$

$$\omega(x) = \omega^1(x) + \psi(x)\omega^2(x) \tag{A.1.2b}$$

where ψ is the sign function used to introduce the discontinuity, defined as

$$\psi(x) = \begin{cases} -1 & \text{if} \quad 0 < x < \frac{L}{2} \\ 1 & \text{if} \quad \frac{L}{2} < x < L \end{cases} \tag{A.1.3}$$

Considering the weighted residual method, the equilibrium equation is multiplied by the test function ω and integrated over the domain:

$$\int_0^L \omega\, \sigma' \, \mathrm{d}x = 0 \tag{A.1.4}$$

From the decomposition of the displacement fields, Eq. (A.1.4) can be cast as

$$\int_0^L (\omega^1 + \psi\omega^2)\sigma' \, \mathrm{d}x = 0, \tag{A.1.5}$$

and taking first ω^1, with $\omega^2 = 0$ and then ω^2, with $\omega^1 = 0$, two variational statements are derived:

$$\int_0^L \omega^1 \sigma' \, \mathrm{d}x = 0 \tag{A.1.6a}$$

$$\int_0^L \psi\omega^2 \sigma' \, \mathrm{d}x = 0 \tag{A.1.6b}$$

Using integration by parts, the Gauss' theorem and the boundary conditions defined by the governing equations in Eq. (A.1.1), two weak forms can be derived, respectively, from Eq. (A.1.6a) and (A.1.6b):

$$\int_0^L (\omega^1)'\sigma \, \mathrm{d}x = 0 \tag{A.1.7a}$$

$$\int_0^L \psi(\omega^2)'\sigma \, \mathrm{d}x = -\int_0^{L/2} \omega^2 \sigma' \, \mathrm{d}x + \int_{L/2}^L \omega^2 \sigma' \, \mathrm{d}x = 2\omega^2(L/2)p \tag{A.1.7b}$$

Indeed, it can be observed that the pressure p only appears in the weak form corresponding to the discontinuous test functions, see Eq. (A.1.7b). This is the expected behaviour because the crack pressure has zero virtual work for continuous virtual displacements.

A.2 Discretisation

The displacement field in Eq. (A.1.2) can be discretised using shape functions as

$$u^1(x) = \sum_{j=1}^{4} u_j^1 N_j(x) = \sum_{j=1}^{4} a_j N_j(x) \tag{A.2.1a}$$

$$u^2(x) = \sum_{j=1}^{4} u_j^2 N_j(x) = \sum_{j=1}^{4} b_j N_j(x) \tag{A.2.1b}$$

$$\omega^1(x) = \omega^2(x) = N_i(x) \tag{A.2.1c}$$

where N_j are the shape functions and a_j and b_j are the nodal displacements associated to u^1 and u^2 respectively.

Considering a local elastic model and the decomposition of u and ω in Eq. (A.1.2) it can be stated that

$$\int_0^L (\omega^1)' \sigma \, \mathrm{d}x = E \int_0^L (\omega^1)' \left((u^1)' + \psi (u^2)' \right) \, \mathrm{d}x = 0 \tag{A.2.2}$$

$$\int_0^L \psi (\omega^2)' \sigma \, \mathrm{d}x = E \int_0^L (\omega^2)' \left(\psi (u^1)' + (u^2)' \right) \, dx = 2\omega^2 (L/2) p, \tag{A.2.3}$$

and using the shape functions defined in Eq. (A.2.1), the discrete weak forms are computed:

$$\mathbf{K_{a,a}}\,\mathbf{a} + \mathbf{K_{a,b}}\,\mathbf{b} = \mathbf{0} \tag{A.2.4a}$$

$$\mathbf{K_{b,a}}\,\mathbf{a} + \mathbf{K_{b,b}}\,\mathbf{b} = \mathbf{f} \tag{A.2.4b}$$

with

$$\mathbf{K_{a,a}} = \mathbf{K_{b,b}} := E \int_0^L \mathbf{N}'^T \mathbf{N}' \mathrm{d}x \tag{A.2.5a}$$

$$\mathbf{K_{a,b}} = \mathbf{K_{b,a}} := E \int_0^L \psi \mathbf{N}'^T \mathbf{N}' \mathrm{d}x \tag{A.2.5b}$$

As discussed in Section A.1, the force vector has zero values in the equation corresponding to the continuous virtual displacements, Eq. (A.2.4a).

Appendix B

Lagrange multipliers

This appendix deals with the treatment of Dirichlet boundary conditions with Lagrange multipliers, see Belytschko et al. (2000). Special attention is given to the treatment of the mechanical and the regularisation boundary conditions.

On the one hand, finite element discretisation of the weak form of the equilibrium and regularisation equations leads to the two discrete weak forms

$$\mathbf{r}_{\text{equil}}(\mathbf{u}, \widetilde{\mathbf{u}}) := \mathbf{f}_{\text{int}}(\mathbf{u}, \widetilde{\mathbf{u}}) - \mathbf{f}_{\text{ext}} = \mathbf{0} \tag{B.0.1a}$$

$$\mathbf{r}_{\text{regu}}(\mathbf{u}, \widetilde{\mathbf{u}}) := -(\mathbf{M} + \ell_c^2 \mathbf{K}_{BC})\mathbf{u} + (\mathbf{M} + \ell_c^2 \mathbf{D})\widetilde{\mathbf{u}} = \mathbf{0} \tag{B.0.1b}$$

On the other hand, the Dirichlet boundary conditions for the mechanical and the regularisation problem, respectively, are defined as

$$\mathbf{A}_{\text{equil}}\mathbf{u} = \mathbf{u}^* \tag{B.0.2a}$$

$$\mathbf{A}_{\text{regu}}\mathbf{u} = \mathbf{A}_{\text{regu}}\widetilde{\mathbf{u}} \quad \Rightarrow \quad \mathbf{A}_{\text{regu}}(\mathbf{u} - \widetilde{\mathbf{u}}) = \mathbf{0} \tag{B.0.2b}$$

Then, the global system can be summarised as

$$\begin{bmatrix} \mathbf{K}_{\mathbf{u},\mathbf{u}} & \mathbf{K}_{\mathbf{u},\tilde{\mathbf{u}}} & | & \mathbf{A}_{\text{equil}}^T & \mathbf{0} \\ \mathbf{K}_{\tilde{\mathbf{u}},\mathbf{u}} & \mathbf{K}_{\tilde{\mathbf{u}},\tilde{\mathbf{u}}} & | & \mathbf{0} & \mathbf{A}_{\text{regu}}^T \\ — & — & — & — & — \\ \mathbf{A}_{\text{equil}} & \mathbf{0} & | & \mathbf{0} & \mathbf{0} \\ \mathbf{A}_{\text{regu}} & -\mathbf{A}_{\text{regu}} & | & \mathbf{0} & \mathbf{0} \end{bmatrix} \begin{bmatrix} \delta\mathbf{u} \\ \delta\tilde{\mathbf{u}} \\ \\ \delta\boldsymbol{\lambda}_{\text{equil}} \\ \delta\boldsymbol{\lambda}_{\text{regu}} \end{bmatrix} = \begin{bmatrix} -\mathbf{r}_{\text{equil}} \\ -\mathbf{r}_{\text{regu}} \\ \\ \mathbf{0} \\ \mathbf{0} \end{bmatrix} \tag{B.0.3}$$

where $\mathbf{A}_{\text{equil}}$ is the matrix of mechanical constraints, $\mathbf{A}_{\text{regu}}$ the matrix of regularisation constraints and

$$\mathbf{K}_{\mathbf{u},\mathbf{u}} = \frac{\partial \mathbf{r}_{\text{equil}}}{\partial \mathbf{u}} \tag{B.0.4a}$$

$$\mathbf{K}_{\mathbf{u},\tilde{\mathbf{u}}} = \frac{\partial \mathbf{r}_{\text{equil}}}{\partial \tilde{\mathbf{u}}} \tag{B.0.4b}$$

$$\mathbf{K}_{\tilde{\mathbf{u}},\mathbf{u}} = \frac{\partial \mathbf{r}_{\text{regu}}}{\partial \mathbf{u}} \tag{B.0.4c}$$

$$\mathbf{K}_{\tilde{\mathbf{u}},\tilde{\mathbf{u}}} = \frac{\partial \mathbf{r}_{\text{regu}}}{\partial \tilde{\mathbf{u}}} \tag{B.0.4d}$$

Note that the global matrix is not symmetric. This is due to the fact that Dirichlet boundary conditions for the regularisation problem tie $\mathbf{u}$ and $\tilde{\mathbf{u}}$.

This method is discussed using a continuous formulation. The same strategy can be extended to a continuous-discontinuous model. For a complete overview of this formulation, see Tamayo-Mas (2013).

Bibliography

Armero, F. and K. Garikipati (1996). An analysis of strong discontinuities in multiplicative finite strain plasticity and their relation with the numerical simulation of strain localization in solids. *International Journal of Solids and Structures 33*(20-22), 2863–2885. doi: 10.1016/0020-7683(95)00257-X.

Bažant, Z. and M. Jirásek (2002). Nonlocal integral formulations of plasticity and damage: Survey of progress. *Journal of Engineering Mechanics 128*(11), 1119–1149. doi: 10.1061/(ASCE)0733-9399(2002)128:11(1119).

Bažant, Z. and B. H. Oh (1983). Crack band theory for fracture of concrete. *Matériaux et Construction 16*(3), 155–177. doi: 10.1007/BF02486267.

Belytschko, T. and T. Black (1999). Elastic crack growth in finite elements with minimal remeshing. *International Journal for Numerical Methods in Engineering 45*(5), 601–620. doi: 10.1002/(SICI)1097-0207(19990620)45:5<601::AID-NME598>3.0.CO;2-S.

Belytschko, T., J. Fish, and B. E. Engelmann (1988). A finite element with embedded localization zones. *Computer Methods in Applied Mechanics and Engineering 70*(1), 59–89. doi: 10.1016/0045-7825(88)90180-6.

Belytschko, T., Y. Krongauz, D. Organ, M. Fleming, and P. Krysl (1996). Meshless methods: An overview and recent developments. *Computer Methods in Applied Mechanics and Engineering 139*(1-4), 3–47. doi: 10.1016/S0045-7825(96)01078-X.

Belytschko, T., W. K. Liu, and B. Moran (2000). *Nonlinear Finite Elements for Continua and Structures*. Wiley.

Bourdin, B., G. A. Francfort, and J. J. Marigo (2000). Numerical experiments in revisited brittle fracture. *Journal of the Mechanics and Physics of Solids 48*(4), 797–826. doi: 10.1016/S0022-5096(99)00028-9.

Comi, C., S. Mariani, and U. Perego (2007). An extended FE strategy for transition from continuum damage to mode I cohesive crack propagation. *International Journal for Numerical and Analytical Methods in Geomechanics 31*(2), 213–238. doi: 10.1002/nag.537.

Crisfield, M. A. (1991). *Non-linear Finite Element Analysis of Solids and Structures. Volume 1: Essentials*. Wiley.

de Borst, R., J. Pamin, R. H. J. Peerlings, and L. J. Sluys (1995). On gradient-enhanced damage and plasticity models for failure in quasi-brittle and frictional materials. *Computational Mechanics 17*(1-2), 130–141. doi: 10.1007/BF00356485.

Francfort, G. A. and J. J. Marigo (1998). Revisiting brittle fracture as an energy minimization problem. *Journal of the Mechanics and Physics of Solids 46*(8), 1319–1342. doi: 10.1016/S0022-5096(98)00034-9.

Herzog, H. (2009). *The Economics and Politics of Climate Change*, Chapter 13: Carbon Dioxide Capture and Storage. Oxford University Press.

Jirásek, M. and M. Bauer (2012). Numerical aspects of the crack band approach. *Computers and Structures 110–111*(0), 60–78. doi: 10.1016/j.compstruc.2012.06.006.

Jirásek, M. and T. Zimmermann (2001). Embedded crack model. Part II: combination with smeared cracks. *International Journal for Numerical Methods in Engineering 50*(6), 1291–1305. doi: 10.1002/1097-0207(20010228)50:6<1291::AID-NME12>3.0.CO;2-Q.

Mazars, J. (1986). A description of micro- and macroscale damage of concrete structures. *Engineering Fracture Mechanics 25*(5–6), 729–737. doi: 10.1016/0013-7944(86)90036-6.

Mazars, J. and G. Pijaudier-Cabot (1996). From damage to fracture mechanics and conversely: A combined approach. *International Journal of Solids and Structures 33*(20–22), 3327–3342. doi: 10.1016/0020-7683(96)00015-7.

Moës, N., J. Dolbow, and T. Belytschko (1999). A finite element method for crack growth without remeshing. *International Journal for Numerical Methods in Engineering 46*(1), 131–150. doi: 10.1002/(SICI)1097-0207(19990910)46:1<131::AID-NME726>3.0.CO;2-J.

Nguyen, V. P., T. Rabczuk, S. Bordas, and M. Duflot (2008). Meshless methods: A review and computer implementation aspects. *Mathematics and Computers in Simulation 79*(3), 763–813. doi: 10.1016/j.matcom.2008.01.003.

Ortiz, M., Y. Leroy, and A. Needleman (1987). A finite element method for localized failure analysis. *Computer Methods in Applied Mechanics and Engineering 61*(2), 189–214. doi: 10.1016/0045-7825(87)90004-1.

Peerlings, R. H. J., R. de Borst, W. A. M. Brekelmans, and M. G. D. Geers (1998). Gradient-enhanced damage modelling of concrete fracture. *Mechanics of Cohesive-frictional Materials 3*(4), 323–342. doi: 10.1002/(SICI)1099-1484(1998100)3:4<323::AID-CFM51>3.0.CO;2-Z.

Rabczuk, T. (2013). Computational Methods for Fracture in Brittle and Quasi-Brittle Solids: State-of-the-Art Review and Future Perspectives. *ISRN Applied Mathematics 2013*, 38 pages. doi: 10.1155/2013/849231.

Rodríguez-Ferran, A., I. Morata, and A. Huerta (2005). A new damage model based on non-local displacements. *International Journal for Numerical and Analytical Methods in Geomechanics 29*(5), 473–493. doi: 10.1002/nag.422.

Simo, J. C. and J. Oliver (1994). A new approach to the analysis and simulation of strain softening in solids. In *Fracture and damage in quasibrittle structures*, pp. 25–39.

Simo, J. C., J. Oliver, and F. Armero (1993). An analysis of strong discontinuities induced by strain-softening in rate-independent inelastic solids. *Computational Mechanics 12*(5), 277–296. doi: 10.1007/BF00372173.

Simone, A., G. N. Wells, and L. J. Sluys (2003). From continuous to discontinuous failure in a gradient-enhanced continuum damage model. *Computer Methods in Applied Mechanics and Engineering 192*(41–42), 4581–4607. doi: 10.1016/S0045-7825(03)00428-6.

Sukumar, N., J. E. Dolbow, and N. Moës (2015). Extended finite element method in computational fracture mechanics: a retrospective examination. *International Journal of Fracture Mechanics 196*, 189–206. doi: 10.1007/s10704-015-0064-8.

Tamayo-Mas, E. (2009). Continuous-discontinuous models of failure based on non-local displacements. Master's thesis, Universitat Politècnica de Catalunya.

Tamayo-Mas, E. (2013). *Continuous-discontinuous modelling for quasi-brittle failure: propagating cracks in a regularised bulk*. Ph. D. thesis, Universitat Politècnica de Catalunya, Departament de Matemàtica Aplicada III.

Tamayo-Mas, E. and A. Rodríguez-Ferran (2013). A new continuous-discontinuous damage model: Cohesive cracks via an accurate energy-transfer process. *Theoretical and Applied Fracture Mechanics* (69), 90–101. doi: 10.1016/j.tafmec.2013.11.009.

Tamayo-Mas, E. and A. Rodríguez-Ferran (2015). A medial-axis-based model for propagating cracks in a regularised bulk. *International Journal for Numerical Methods in Engineering 101*, 489–520. doi: 10.1002/nme.4757.

Wells, G. N., L. J. Sluys, and R. de Borst (2002). Simulating the propagation of displacement discontinuities in a regularized strain-softening medium. *International Journal for Numerical Methods in Engineering 53*(5), 1235–1256. doi: 10.1002/nme.375.